IAEA
International Atomic Energy Agency

INDC(IND)-0049
Distr. G

INDC International Nuclear Data Committee

Measurements of neutron capture cross sections on ^{70}Zn at 0.96 and 1.69 MeV

B. Lalremruata[1], L.R.M. Punte[1], N. Otuka[2], Rebecca Pachuau[1], Y. Iwamoto[3], S.V. Suryanarayana[4], B.K. Nayak[4], B. Satheesh[1], H.H. Thanga[1], L.S. Danu[4], V.V. Desai[4], L.R. Hlondo[1], S. Kailas[4], S. Ganesan[5], A. Saxena[4]

[1]Department of Physics, Mizoram University, Tanhril, Aizawl, India
[2]Nuclear Data Section, International Atomic Energy Agency, Wien, Austria
[3]Japan Atomic Energy Agency, Tokai-mura, Naka-gun, Ibaraki, Japan
[4]Nuclear Physics Division, BARC, Mumbai, India
[5]Reactor Physics Design Division, BARC, Mumbai, India

March 2017

Selected INDC documents may be downloaded in electronic form from
http://www-nds.iaea.org/publications/
or sent as an e-mail attachment.
Requests for hardcopy or e-mail transmittal should be directed to
nds.contact-point@iaea.org
or to:

Nuclear Data Section
International Atomic Energy Agency
Vienna International Centre
PO Box 100
A-1400 Vienna
Austria

Produced by the IAEA in Austria
March 2017

INDC (IND)-0049
Distr. G

Measurements of neutron capture cross sections on 70Zn at 0.96 and 1.69 MeV

B. Lalremruata[1], L.R.M. Punte[1], N. Otuka[2], Rebecca Pachuau[1], Y. Iwamoto[3], S.V. Suryanarayana[4], B.K. Nayak[4], B. Satheesh[1], H.H. Thanga[1], L.S. Danu[4], V.V. Desai[4], L.R. Hlondo[1], S. Kailas[4], S. Ganesan[5], A. Saxena[4]

[1]Department of Physics, Mizoram University, Tanhril, Aizawl, India
[2]Nuclear Data Section, International Atomic Energy Agency, Wien, Austria
[3]Japan Atomic Energy Agency, Tokai-mura, Naka-gun, Ibaraki, Japan
[4]Nuclear Physics Division, BARC, Mumbai, India
[5]Reactor Physics Design Division, BARC, Mumbai, India

March 2017

Abstract

The cross sections of the $^{70}Zn(n,\gamma)^{71}Zn^{m}$ ($T_{1/2}$ = 3.96±0.05 hrs) reaction have been measured relative to the $^{197}Au(n,\gamma)^{198}Au$ cross sections at 0.96 and 1.69 MeV using a $^{7}Li(p,n)^{7}Be$ neutron source and activation technique. The cross section of this reaction has been measured for the first time in the MeV region. The new experimental cross sections have been compared with the theoretical prediction by TALYS-1.6 with various level density models as well as the TENDL-2015 library. The generalized superfluid level density model predicted the new experimental cross sections at both incident energies. The $^{70}Zn(n,\gamma)^{71}Zn^{g+m}$ total capture cross sections have also been derived by applying the evaluated isomeric ratios in the TENDL-2015 library to the measured partial capture cross sections. The spectrum averaged total capture cross sections derived in the present work agree well with the JENDL-4.0 library at 0.96 MeV whereas it lies between the TENDL-2015 and JENDL-4.0 libraries at 1.69 MeV. This experimental work has been also published as Phys. Rev. C 95 (2017) 024619.

Measurements of neutron capture cross sections on ^{70}Zn at 0.96 and 1.69 MeV

B. Lalremruata[1,*], L.R.M. Punte[1], N. Otuka[2], Rebecca Pachuau[1], Y. Iwamoto[3], S.V. Suryanarayana[4], B.K. Nayak[4], B. Satheesh[1], H.H. Thanga[1], L.S. Danu[4], V.V. Desai[4], L.R. Hlondo[1], S. Kailas[4], S. Ganesan[5], A. Saxena[4]

[1]Department of Physics, Mizoram University, Tanhril - 796004, India

[2]Nuclear Data Section, International Atomic Energy Agency, A-1400, Wien, Austria

[3]Japan Atomic Energy Agency, Tokai-mura, Naka-gun, Ibaraki, 319-1195 Japan

[4]Nuclear Physics Division, BARC, Mumbai - 40085, India

[5]Reactor Physics Design Division, BARC, Mumbai - 40085, India

Abstract - The cross sections of the ^{70}Zn(n,γ)^{71}Zn^{m} ($T_{1/2}$ = 3.96±0.05 hrs) reaction have been measured relative to the ^{197}Au(n,γ)^{198}Au cross sections at 0.96 and 1.69 MeV using a ^{7}Li(p,n)^{7}Be neutron source and activation technique. The cross section of this reaction has been measured for the first time in the MeV region. The new experimental cross sections have been compared with the theoretical prediction by TALYS-1.6 with various level density models as well as the TENDL-2015 library. The generalized superfluid level density model predicted the new experimental cross sections at both incident energies. The ^{70}Zn(n,γ)^{71}Zn^{g+m} total capture cross sections have also been derived by applying the evaluated isomeric ratios in the TENDL-2015 library to the measured partial capture cross sections. The spectrum averaged total capture cross sections derived in the present work agree well with the JENDL-4.0 library at 0.96 MeV whereas it lies between the TENDL-2015 and JENDL-4.0 libraries at 1.69 MeV. This experimental work has been also published as Phys. Rev. C 95 (2017) 024619.

PACS number(s): 25.40.Lw, 21.10.Ma, 25.60.Dz

*Corresponding author: B. Lalremruata (marema08@gmail.com)

1. INTRODUCTION:

The neutron capture cross sections of the zinc isotopes are important both for reactor applications as well as for nuclear astrophysics. These cross sections in the energy region relevant to the s-process were not known accurately. In order to improve the situation, Reifarth et al. [1] performed an experiment to study the Maxwellian averaged cross sections (MACS) of ^{64}Zn, ^{68}Zn and ^{70}Zn neutron captures at kT = 25 keV, which concludes that the ^{70}Zn neutron capture MACS is about half of the value recommended by Bao et al. [2] though it does not have a strong impact on the s-process scenario. This neutron capture reaction is also a candidate of dosimetry reactions to study deviation of the epithermal reactor neutron spectrum from 1/E distribution [3]. Except for the thermal neutron energy, the above mentioned kT ~ 25 keV spectrum averaged cross section is the unique experimental ^{70}Zn neutron capture cross section available in the EXFOR library [4], while comparison of evaluated cross sections in the TENDL-2015 [5], JENDL-4.0 [6,7] and EAF-2010 [8] libraries shows large discrepancies between the upper boundary of the resolved resonance region and 10 MeV. The purpose of this paper is to report new ^{70}Zn(n,γ)^{71}Zn^{m} (3.96 ± 0.05 hrs) cross sections experimentally determined at incident neutron energies of 0.96 and 1.69 MeV to achieve improvement in our knowledge of this capture reaction in the fast neutron region.

2. EXPERIMENTAL DETAILS:

2.1. Neutron source:

The experiment was performed at the Folded Tandem Ion Accelerator (FOTIA) Facility, Nuclear Physics Division, Bhabha Atomic Research Centre (BARC), Mumbai. The protons at 2.80 and 3.50 MeV after passing through a beam collimator (0.5 cm in diameter) bombarded a 2.0-mg/cm^2 (37.4 μm) thick natural lithium target to produce neutrons through the ^{7}Li(p,n)^{7}Be reaction (E_{th} = 1.881 MeV). The proton beam energy spread is ±0.02 MeV. A fresh lithium target was used for irradiation at each proton energy. The lithium targets were supplied by the

Tata Institute of Fundamental Research (TIFR), Mumbai, and prepared using the rolling method at TIFR. A 0.25-mm thick tantalum foil (manufactured by Goodfellow Cambridge Limited, England, and supplied by H. Fillunger & Co. Pvt. Ltd., Banglore) on which the lithium target was pasted was used as a proton beam stopper. The proton beam current during irradiation varied from 50 to 100 nA, and the beam diameter on the lithium target was about 5 mm. The neutron flux was monitored online by a NE213 neutron detector at zero degree and at 1 m distance from the lithium target. The neutron flux was recorded and saved every 30 minutes to get the neutron flux fluctuation during the whole irradiation period.

The proton beam was continuous, and therefore TOF technique cannot be employed to measure the neutron flux energy spectrum. We therefore rely on the $^{7}Li(p,n)^{7}Be$ neutron flux energy spectrum code EPEN [9] developed at our laboratory to obtain the neutron flux energy spectra $\varphi(E)$ for various lithium target configurations based on the $^{7}Li(p,n)^{7}Be$ cross section evaluated by H. Liskien and A. Paulsen [10]. The neutron flux energy spectra $\varphi(E)$ calculated by EPEN at the two proton energies in the present experimental configuration are shown in **Figs. 1 and 2**. It can be seen that the neutron energy is quasi-monoenergetic due to the proton energy loss in the lithium target and also due to the finite angular coverage of the neutron capture reaction target in the experimental setup. Since the proton energies in the present experiment are above the threshold energy of the $^{7}Li(p,n_1)^{7}Be$ reaction (2.37 MeV), there are (p,n_1) low energy background neutrons in addition to the (p,n_0) neutrons, and their contribution should be known for subtraction. The mean energy of the (p,n_0) neutron group was obtained by

$$<E_n> = \int\varphi_0(E)\, E\, dE \,/\, \int\varphi_0(E)\, dE \qquad (1)$$

with the EPEN (p,n_0) neutron flux energy spectrum $\varphi_0(E)$, and it is 0.96 and 1.69 MeV for E_p=2.80 and 3.50 MeV, respectively. The width of the (p,n_0) spectrum is ±0.15 MeV at both proton energies. The neutron flux energy spectra plotted in Figs. 1 and 2 are also tabulated in **Appendix A**.

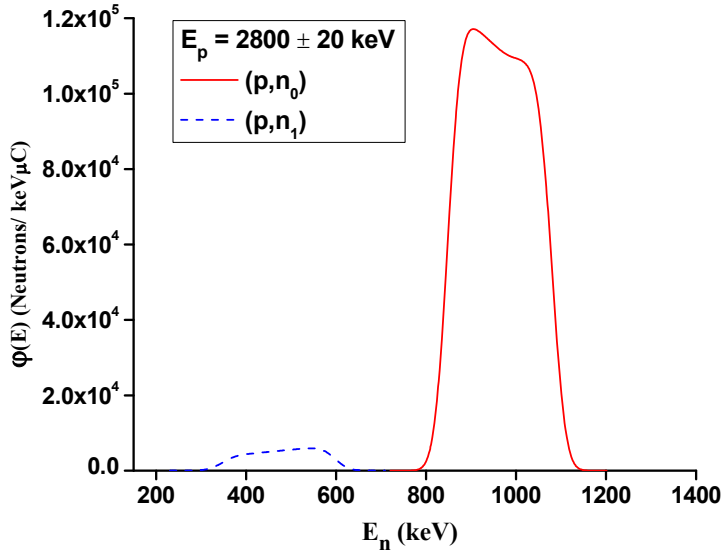

Fig. 1: Neutron flux energy spectrum φ(E) from the $^{7}Li(p,n_0)^{7}Be$ and $^{7}Li(p,n_1)^{7}Be$ reaction at E_p = 2.80±0.02 MeV obtained from the code EPEN.

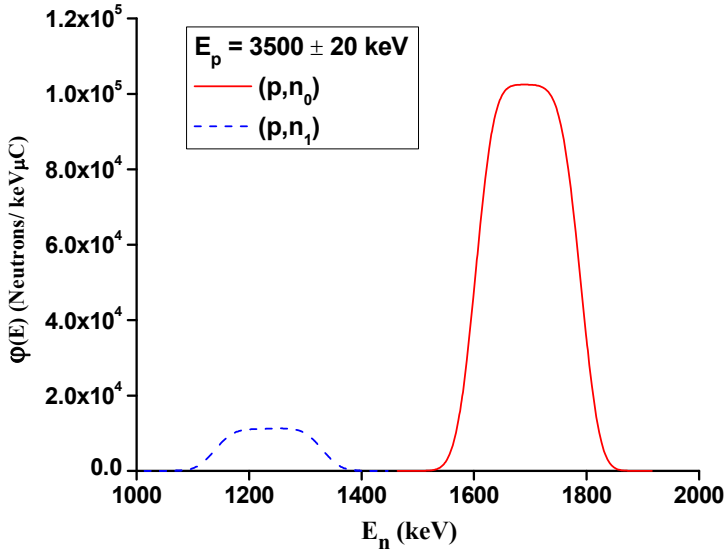

Fig. 2: Neutron flux energy spectrum φ(E) from the $^{7}Li(p,n_0)^{7}Be$ and $^{7}Li(p,n_1)^{7}Be$ reaction at E_p = 3.50±0.02 MeV obtained from the code EPEN.

2.2. Sample preparation:

A zinc foil enriched (72.4±1.0%) to ^{70}Zn (manufactured by FUSE "Integrated Plant Electrohimpribor", Russia, and supplied by AMT Ventures Pvt. Ltd.) was sandwiched between gold foils (manufactured by Goodfellow Cambridge Limited, England, and supplied by H. Fillunger & Co. Pvt. Ltd., Banglore). The gold foils were used for normalization of the measured cross section with the ^{197}Au(n,γ)^{198}Au standard cross section. Furthermore, another natural indium foil (provided by BARC) was stacked at the end of the foil stack to serve as an independent flux monitor foil using the ^{115}In(n,n')^{115}In^{m} reaction for cross-checking. The whole stacked foils (10 mm × 10 mm) were wrapped with a 0.025 mm-thick superpure aluminium foil. The Au-Zn-Au-In stack was mounted at zero degree with respect to the beam direction at a distance of 14 mm from the lithium target. All foils were weighted at TIFR with an accuracy of 0.1 mg. Details about the foils used in the experiment are given in **Table 1**. The experimental setup is schematically shown in **Fig. 3**.

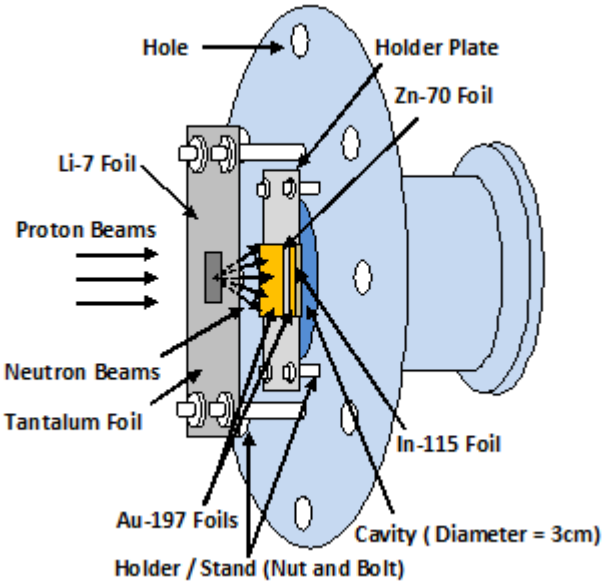

Fig. 3: The schematic diagram of the experimental setup.

Table 1: Details of foils used in the present experiment.

Isotope	Enrichment (%)	Purity (%)	E_n (MeV)	Thickness (mg/cm^2)	Number of atoms of the isotope (10^{-4}atoms/b)
^{70}Zn	72.4±1.0 8.49 (^{64}Zn) 8.40 (^{66}Zn) 2.01 (^{67}Zn) 8.70 (^{68}Zn)	>99.97	0.96	87.3±0.1	5.529
			1.69	113.6±0.1	7.194
^{197}Au	100%	99.95	0.96	72.3±0.1 (front) 68.5±0.1 (back)	2.211 (front) 2.094 (back)
			1.69	74.0±0.1 (front) 70.3±0.1 (back)	2.263 (front) 2.149 (back)
^{115}In	95.71%	99.99	0.96	102.0±0.1	5.120
			1.69	129.8±0.1	6.516

2.3. Measurement of *γ* -ray activity:

After completion of the neutron irradiation and sufficient cooling, the foil stack was transferred to the counting room. The γ-ray activity was measured using a pre-calibrated lead-shielded 185 cc high purity germanium (HPGe) detector having 30% relative efficiency, and 1.8 keV energy resolution at 1.33 MeV γ-energy. The data acquisition was carried out using CAMAC based LAMPS (Linux Advanced Multi Parameter System) software (TCAMCON-95/CC 2000 crates controller and CM-48 ADCs). Therefore, the detector dead time was negligible. To correctly identify the γ-ray of interest, the decay curve analysis was carried out by saving the γ count periodically as shown in **Table 2** and followed for 2 – 3 times the half-life of $^{71}Zn^{m}$. Details of decay data adopted in the analysis are given in **Table 3**. A typical γ-ray spectrum of the present experiment at $<E_n>$= 1.69 MeV is shown in **Fig. 4**.

Table 2: Irradiation, cooling and counting times.

E_n (MeV)	Irradiation time (sec.)	Run No.	Cooling time (sec.) (beam stop time-counting start time)	Counting time (sec.)
0.96	26580.0	1	1808.0	3875.6
		2	5705.6	3636.9
		3	9373.5	7313.7
		4	16746.2	7212.3
		5	24012.5	1836.0
1.69	30300.0	1	1534.0	3591.2
		2	5180.2	3634.3
		3	8851.5	3616.9
		4	12541.4	7253.3
		5	20113.7	10368.6
		6	30573.3	7950.3
		7	38531.6	6353.3

Table 3: Decay data adopted in the present work taken from the ENSDF library [11-13].

Nuclide	Half-life	E_γ (keV)	I_γ (%)
$^{71}Zn^m$	3.96 ± 0.05 h	386.280	91.40±2.10
^{198}Au	2.6947 ± 0.0003 d	411.802	95.62±0.06
$^{115}In^m$	4.486 ± 0.004 h	336.240	45.80±2.20

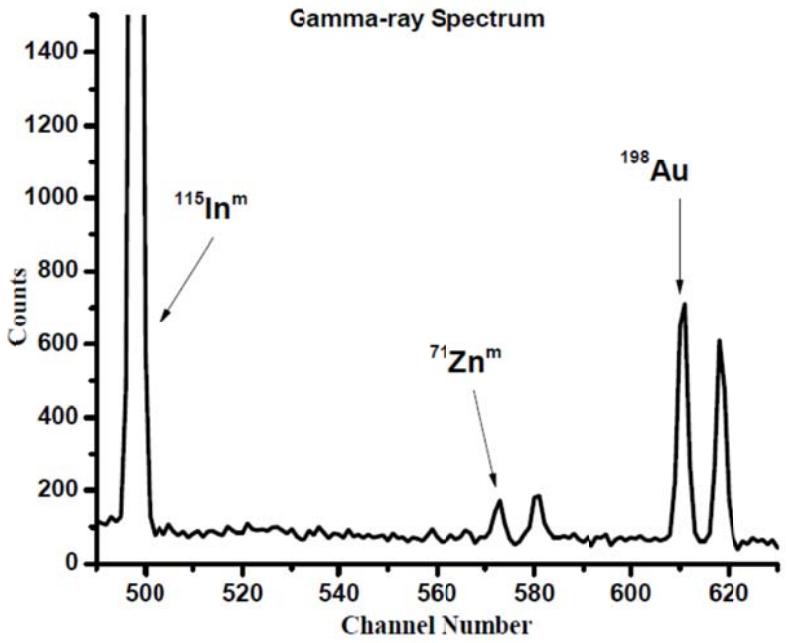

Fig. 4: Typical γ-ray spectrum of radioactive nuclides $^{115}In^m$, $^{71}Zn^m$ and ^{198}Au at $<E_n>$=1.69 MeV.

2.4. HPGe detector efficiency calibration:

A ^{152}Eu point source ($T_{1/2}$ = 13.517 years [14]) of known activity (A_0 = 7582.5 Bq on 1st Oct. 1999) was used for determination of the absolute photo peak efficiency of the HPGe detector at various characteristic γ energies of the point source. The detection efficiency for the point source placed at a distance of 1 cm from the detector ε_p was determined by

$$\varepsilon_p = \varepsilon_G \, C \, K_c / (A_0 \, e^{-\lambda t} \, \Delta t \, I_\gamma) \quad (2)$$

where C is the number of counts during the counting time (Δt = 3607 sec), A_0 is the ^{152}Eu source activity at the time of manufacture, t is the time elapsed from the date of manufacturer to the start time of counting, λ is the decay constant, I_γ is the decay γ intensity, and K_c is the correction factor for the coincidence summing effect. The geometric efficiency $\varepsilon_G = \Delta\Omega/4\pi$, where $\Delta\Omega = 2\pi\,[1-d/(d^2+r^2)^{1/2}]$ for detector having the source-to-detector distance d and detector radius r.

Since the count rate from the $^{70}Zn(n,\gamma)^{71}Zn^m$ reaction is rather low, we needed to place the foil stack very close to the detector to obtain high count rate. Therefore the efficiency calibration source had also to be placed at the same distance, which is 1 cm from the detector. However, this introduces the coincidence-summing effect. Evaluations of the coincidence summing effect and detection efficiency are discussed in the following sections. Note that all parameters independent of γ energies are finally cancelled because we need only the ratio of detection efficiencies in the determination of the cross sections.

2.4.1. Coincidence Summing Effect:

When two γ-rays emitted in a cascade are detected within the resolving time of the detector, the detector cannot distinguish between the two γ-rays, and thus giving rise to a single signal in the spectrum as if a single γ-ray would have been detected. This is known as “cascade” or “true coincidence” summing. This leads to (1) a loss in count (“summed out”) from the peaks corresponding to two γ-rays, and (2) an addition of count (“summed in”) at the sum of two energies. For any source-to-detector distance there will be some degree of summing depending

on the detector size, beyond a certain distance, coincidence-summing losses will be negligible [15].

Table 4 shows the ^{152}Eu standard source characteristic γ energies and their corresponding γ intensities considered in the detector efficiency measurement. In order to correct the measured efficiency for the coincidence summing effect, the correction factor K_c was calculated using the Monte Carlo simulation code EFFTRAN [16]. The detector efficiencies with and without the correction measured at the characteristic γ energies of the ^{152}Eu point source are shown in **Fig. 5**. Only the efficiency ratio is necessary for determination of the cross sections, and therefore only the uncertainties in counting statistics and γ intensity were considered in the error propagation to the efficiencies of the $^{71}Zn^{m}$ and ^{198}Au characteristic γ lines.

Since the calibration of the HPGe detector was carried out with the point source while the activated foil stack has finite area (1 cm × 1 cm), the efficiency for the point source geometry ε_p was transferred by EFFTRAN to the efficiency for the foil stack geometry ε, which is shown in **Fig. 6** and Table 4.

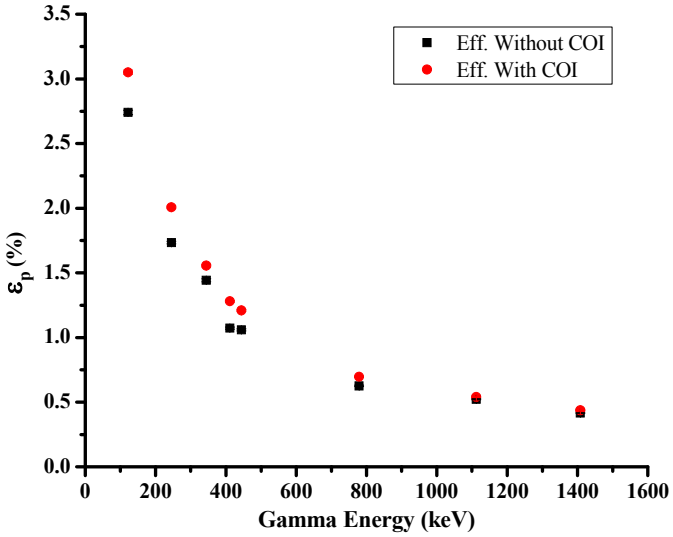

Fig. 5: Experimental detection efficiency of the HPGe detector ε_p for the ^{152}Eu standard point sources placed at distance of 1 cm from the detector with and without true coincidence summing corrections (COI). The error bar for the uncertainty due to counting statistics is within the symbol.

Table 4: Detection efficiencies for the point source geometry ε_p and for the foil stack geometry ε at the characteristic γ energies of ^{152}Eu with their γ intensities I_γ [14] adopted for efficiency determination, counts C and coincidence summing effect correction factors K_c. The 444.0 keV γ line consists of 443.96 keV (I_γ=2.827±0.014%) and 444.01 keV (I_γ=0.298±0.011%) unresolved by our detector. The uncertainty in ε is propagated from the uncertainties in C and I_γ.

E_γ (keV)	I_γ (%)	C	K_c	ε_p	ε
121.8	28.53±0.16	328049.3	1.113	3.0514	3.0270±0.0178
244.7	7.55±0.04	53997.8	1.158	2.0083	1.9940±0.0136
344.3	26.59±0.20	157183.5	1.078	1.5550	1.5450±0.0123
411.1	2.237±0.013	9647.2	1.193	1.2803	1.2720±0.0149
444.0	3.125±0.018	13292.1	1.142	1.2087	1.2013±0.0125
778.9	12.93±0.08	32542.8	1.112	0.6964	0.6922±0.0058
1112.1	13.67±0.08	28712.2	1.033	0.5399	0.5368±0.0045
1408.0	20.87±0.09	34940.8	1.050	0.4374	0.4349±0.0030

2.4.2. Interpolation of Detection Efficiency:

In order to obtain the detector efficiencies at the characteristic γ energies of the $^{70}Zn^{m}$ (E_{Zn}=386.28 keV) and ^{198}Au (E_{Au}=411.802 keV), the point-wise efficiencies in Table 4 were interpolated through the following fitting function:

$$\varepsilon (E) = \varepsilon_0 \exp (-E/E_0) + \varepsilon_c \qquad (3)$$

The fitting parameter values are given in **Table 5**. This curve gives the detection efficiencies of 386.28 keV γ-ray of $^{71}Zn^{m}$ and 411.802 keV γ-ray of ^{198}Au as ε_{Zn}=1.404644 ± 0.034969% and ε_{Au}=1.319418 ± 0.034688%, respectively. The covariance between two interpolated efficiencies ε_{Zn} and ε_{Au} are obtained following the prescription by Mannhart [17]:

$$\begin{aligned}\mathrm{cov}(\varepsilon_{Zn}, \varepsilon_{Au}) = {} & \exp[-(E_{Zn}+E_{Au})/E_0](\Delta\varepsilon_0)^2 \\ & + (\varepsilon_0^2 E_{Zn}E_{Au}/E_0^4)\exp[-(E_{Zn}+E_{Au})/E_0](\Delta E_0)^2 \\ & + (\Delta\varepsilon_c)^2 \\ & + \varepsilon_0[(E_{Zn}+E_{Au})/E_0^2]\exp[-(E_{Zn}+E_{Au})/E_0]\,\mathrm{cov}(E_0, \varepsilon_0) \\ & + [\exp(-E_{Zn}/E_0) + \exp(-E_{Au}/E_0)]\,\mathrm{cov}(\varepsilon_0, \varepsilon_c) \\ & + [(\varepsilon_0 E_{Zn}/E_0^2)\exp(-E_{Zn}/E_0) + (\varepsilon_0 E_{Au}/E_0^2)\exp(-E_{Au}/E_0)]\,\mathrm{cov}(\varepsilon_c, E_0) \qquad (4),\end{aligned}$$

with $(\Delta\varepsilon_{Zn})^2 = \mathrm{var}(\varepsilon_{Zn})$ and $(\Delta\varepsilon_{Au})^2 = \mathrm{var}(\varepsilon_{Au})$. This is further propagated to the uncertainty in the detector efficiency ratio $\eta = \varepsilon_{Zn}/\varepsilon_{Au}$,

$$(\Delta\eta/\eta)^2 = (\Delta\varepsilon_{Zn}/\varepsilon_{Zn})^2 + (\Delta\varepsilon_{Au}/\varepsilon_{Au})^2 - 2\,\mathrm{cov}(\varepsilon_{Zn},\varepsilon_{Au})/(\varepsilon_{Zn}\,\varepsilon_{Au}), \qquad (5)$$

and we finally obtain $\eta = 1.06459 \pm 0.00274$.

Table 5: The efficiency curve fitting parameter values.

Parameter	Value	Uncertainty	Correlation coefficient		
ε_0	3.889	0.2083	1.000		
E_0 (keV)	279.541	16.880	-0.843	1.000	
ε_c	0.428	0.0194	0.408	-0.687	1.000

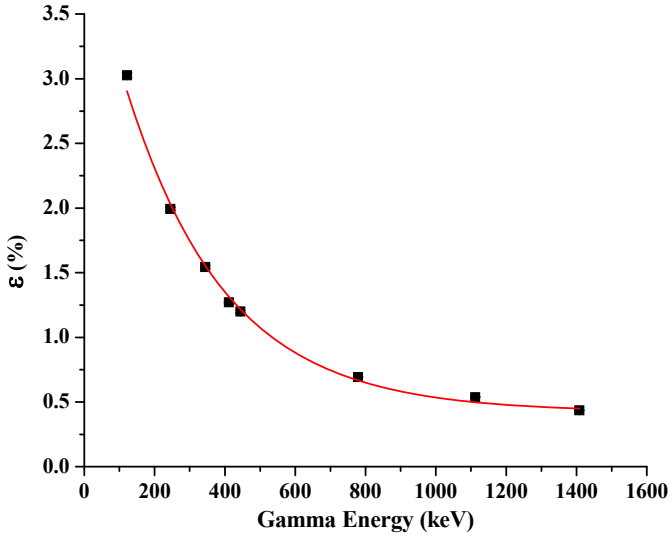

Fig. 6: Detection efficiency calibration curve of the HPGe detector for the 1 cm ×1 cm source placed at a distance of 1 cm from the detector. The error bar for the uncertainty due to counting statistics is within the symbol.

3. DATA ANALYSIS PROCEDURE:

3.1. Estimation of the cross section and its uncertainty:

The measured $^{70}Zn(n,\gamma)^{71}Zn^m$ cross section $<\sigma_{Zn}^m>_{exp}$ was derived with the $^{197}Au(n,\gamma)^{198}Au$ reference cross section $<\sigma_{Au}>$ by

$$<\sigma_{Zn}^m>_{exp} = <\sigma_{Au}>(A_{Zn}/A_{Au})\,[(a_{Au}N_{Au}I_{Au}\varepsilon_{Au}f_{Au})/(a_{Zn}N_{Zn}I_{Zn}\varepsilon_{Zn}f_{Zn})]\,(C_{Zn}/C_{Au}), \quad (6)$$

where $A_x=\Sigma_i A_{x,i}$ is the number of counts ($A_{x,i}$ is the number of counts from i-th counting), a_x is the isotopic abundance of the sample, N_x is the number of atoms, I_x is the γ intensity, ε_x is the detection efficiency,

$$f_x=[1-\exp(-\lambda_x t_1)]\,\Sigma_i \exp(-\lambda_x t_{2,i})\,[1-\exp(-\lambda_x t_{3,i})]\,/\lambda_x \quad (7)$$

is the timing factor for the irradiation time t_1, cooling time for the i-th counting $t_{2,i}$, measuring time for the i-th counting $t_{3,i}$, λ_x is the decay constant, and C_x is the correction factor (x=Zn or Au). See Tables 2 and 3 for timing parameters and decay data, respectively. The symbol <...> signifies that the cross section is averaged for the (p,n_0) neutron flux energy spectrum $\varphi_0(E)$. The fractional uncertainty in the cross section was estimated by the quadrature sum of the fractional uncertainty in $<\sigma_{Au}>$, A_x, a_x, N_x, I_x, f_x, C_x (x=Zn and Au) as well as $\varepsilon_{Au}/\varepsilon_{Zn}$. The fractional uncertainty in $\Delta f_x/f_x$ was determined assuming that the uncertainty is due to the uncertainty in the half-lives of ^{71m}Zn and ^{198}Au. See **Appendix B** for the determination of $\Delta f_x/f_x$.

3.2 Reference cross section:

The reference cross section $<\sigma_{Au}>$ was obtained by folding the IAEA Neutron Cross-Section Standards $\sigma_{Au}(E)$ [18] with the neutron flux energy spectrum $\varphi_0(E)$ obtained by EPEN:

$$<\sigma_{Au}> = \int\varphi_0(E)\,\sigma_{Au}(E)\,dE \,/\, \int\varphi_0(E)\,dE \quad (8).$$

The energy integrated neutron flux determined from the ^{198}Au activity after subtracting the contributions of (p,n_1) neutrons is ~ 1.2×10^6 n/cm^2/s at 0.96 MeV and ~ 1.4×10^6 n/cm^2/s at 1.69 MeV. These fluxes agree well with those determined by the measured $^{115}In^m$ counts and the

evaluated $^{115}In(n,n')^{115}In^{m}$ cross section in the IRDF-2002 library [19] within 5%. The uncertainty in $<\sigma_{Au}>$ due to the uncertainty in the IAEA Neutron Cross-Section Standards was obtained by

$$(\Delta<\sigma_{Au}>)^2 = \Sigma_i [\Phi_i^2 \text{ var } (<\sigma_i>)] / (\Sigma_i \Phi_i)^2 + 2 \Sigma_{i>j} [\Phi_i \Phi_j \text{ cov } (<\sigma_i>, <\sigma_j>)] / (\Sigma_i \Phi_i)^2, \quad (9)$$

where cov $(<\sigma_i>, <\sigma_j>)$ and var $(<\sigma_i>)$ are the covariance between the i-th and j-th group-wise cross section compiled in the IAEA Neutron Cross-Section Standards and its diagonal component (i=j), and $\Phi_i = \int_i \varphi_0(E)\, dE$ is the neutron flux energy spectrum integrated over the i-th group of the IAEA Neutron Cross-Section Standards. The summations for i and j are taken for all energy groups between 0.675 and 1.325 MeV for $<E_n>$=0.96 MeV neutrons (11 groups), and between 1.325 and 2.100 MeV for $<E_n>$=1.69 MeV neutrons (4 groups). In order to obtain the absolute covariance for the IAEA Neutron Cross-Section Standards, the relative covariance ($\%^2$) compiled in the ENDF-6 format was converted to the corresponding absolute covariance (b^2) by multiplying the unweighted group-wise cross section $<\sigma_i>$ constructed by ourselves. The spectrum averaged cross sections are $<\sigma_{Au}>$=82.77 ± 0.86 mb at 0.96 MeV and 64.09 ± 0.92 mb at 1.69 MeV. The fractional group-wise flux $\Phi_i/\Sigma\Phi_i$, group-wise cross sections $<\sigma_i>$, and their correlation coefficients

$$\text{cor}(<\sigma_i>, <\sigma_j>) = \text{cov } (<\sigma_i>, <\sigma_j>) / [\text{var } (<\sigma_i>) \text{ var } (<\sigma_j>)]^{1/2} \quad (10)$$

at 0.96 and 1.69 MeV are given in **Tables 6 and 7**, respectively.

Similarly the covariance between two spectrum averaged cross sections at 0.96 and 1.69 MeV is obtained by $\Sigma_{i,j} [\Phi_i \Phi_j \text{ cov } (<\sigma_i>, <\sigma_j>)] / (\Sigma_i \Phi_i) (\Sigma_j \Phi_j)$, where the summation for i is taken for all energy groups between 0.675 and 1.325 MeV for $<E_n>$=0.96 MeV neutrons while the summation for j is taken for all energy groups between 1.325 and 2.100 MeV for $<E_n>$=1.69 MeV neutrons. By using the correlation coefficients cor$(<\sigma_i>, <\sigma_j>)$ in **Table 8**, we obtain 0.059 mb^2 as the covariance of the spectrum averaged cross sections between two energies. These results are also summarized in **Table 9**.

Table 6. The fractional group-wise flux $\Phi_i/\Sigma\Phi_i$ of the $^7Li(p,n_0)^7Be$ spectrum, unweighted group-wise cross section $<\sigma_i>$ and correlation coefficient cor($<\sigma_i>$, $<\sigma_j>$) in the IAEA Neutron Cross-Section Standards for $<E_n>$=0.96 MeV neutrons.

E_{min} (MeV)	E_{max} (MeV)	$\Phi_i/\Sigma\Phi_i$	$<\sigma_i>$ (b)	$\Delta<\sigma_i>$ (%)	cor($<\sigma_i>$, $<\sigma_j>$) × 100										
0.675	0.725	5.7302E-10	0.0964	1.1287	100.000										
0.725	0.775	2.7463E-05	0.0932	1.2969	43.900	100.000									
0.775	0.825	9.6409E-03	0.0891	1.0479	34.120	51.770	100.000								
0.825	0.875	1.2307E-01	0.0859	1.6264	20.010	28.920	33.310	100.000							
0.875	0.920	1.9745E-01	0.0849	2.1847	13.070	11.730	12.760	10.720	100.000						
0.920	0.950	1.3143E-01	0.0851	1.9326	6.647	12.920	24.510	15.210	8.827	100.000					
0.950	0.970	8.5593E-02	0.0854	4.2426	2.581	4.046	5.590	9.520	3.219	6.007	100.000				
0.970	0.990	8.4304E-02	0.0841	3.1765	7.715	6.316	7.412	6.074	43.520	4.910	1.937	100.000			
0.990	1.050	2.4379E-01	0.0808	1.0412	18.680	15.450	24.820	25.120	20.390	38.090	11.400	11.690	100.000		
1.050	1.175	1.2469E-01	0.0773	1.3918	16.260	14.120	13.780	12.560	13.200	21.030	7.447	9.168	44.870	100.000	
1.175	1.325	2.8842E-07	0.0740	1.2621	17.280	16.130	18.170	12.910	11.790	6.297	3.395	12.260	27.560	40.740	100.000

Table 7. The fractional group-wise flux $\Phi_i/\Sigma\Phi_i$ of the $^7Li(p,n_0)^7Be$ spectrum, unweighted group-wise cross section $<\sigma_i>$ and correlation coefficient cor($<\sigma_i>$, $<\sigma_j>$) in the IAEA Neutron Cross-Section Standards for $<E_n>$=1.69 MeV neutrons.

E_{min} (MeV)	E_{max} (MeV)	$\Phi_i/\Sigma\Phi_i$	$<\sigma_i>$ (b)	$\Delta<\sigma_i>$ (%)	cor($<\sigma_i>$, $<\sigma_j>$) × 100			
1.325	1.500	1.0181E-06	0.0708	1.7245	100.000			
1.500	1.700	5.2954E-01	0.0666	1.5090	34.570	100.000		
1.700	1.900	4.7046E-01	0.0600	2.0399	15.280	37.460	100.000	
1.900	2.100	3.0301E-08	0.0521	1.6346	12.010	25.040	38.210	100.000

Table 8. The correlation coefficient cor($<\sigma_i>$, $<\sigma_j>$) in the IAEA Neutron Cross-Section Standards between $<E_n>$=0.96 and 1.69 MeV neutrons.

	E_{min} (MeV)	E_{max} (MeV)	cor($<\sigma_i>$, $<\sigma_j>$) × 100										
E_{min} (MeV)			0.675	0.725	0.775	0.825	0.875	0.920	0.950	0.970	0.990	1.050	1.175
E_{max} (MeV)			0.725	0.775	0.825	0.875	0.920	0.950	0.970	0.990	1.050	1.175	1.325
	1.325	1.500	11.87	10.39	12.03	9.145	8.119	10.56	6.673	6.962	15.54	17.22	39.12
	1.500	1.700	14.01	12.28	14.40	11.14	10.95	10.76	4.417	8.172	18.60	14.93	22.76
	1.700	1.900	10.34	9.03	10.71	8.154	9.124	7.886	6.538	7.369	13.89	10.68	12.57
	1.900	2.100	12.09	10.5	12.47	9.483	10.09	9.439	4.228	7.915	16.07	12.78	14.88

Table 9. Reference cross section $<\sigma_{Au}>$ with their uncertainty and correlation coefficient.

E_n (MeV)	Value (mb)	Uncertainty (mb)	Correlation coefficient	
0.96	82.77	0.86	1.00	
1.69	64.09	0.92	0.07	1.00

3.3 Corrections:

The correction factor C_x in Eq. (6) is decomposed to

$$C_x = C_{x,fluc} \cdot C_{x,low} \cdot C_{x,scat} \cdot C_{x,attn} \qquad (11)$$

(x = Zn or Au). Each term is the correction factor for

1. neutron flux fluctuation (fluc)
2. low energy neutron backgrounds due to $^7Li(p,n_1)^7Be$ neutrons (low)
3. scattered neutron background originating from elastic, inelastic and multiple scattering in the foil stack and the surrounding materials (scat)
4. γ-rays self-attenuation (attn).

and summarized in **Table 10.** Some correction factors were determined for the two gold foils separately and their means were applied to Eq. (6) because we did not count γ-rays from two gold foils separately.

Table 10: Correction factors applied to the measured cross section derivation by Eq.(6).

E_n (MeV)	0.96	1.69
$C_{Zn,fluc}/ C_{Au,fluc}$	0.869	0.748
$C_{Au,low}$	0.920 (front) 0.921 (back) 0.921 (mean)	0.884 (front) 0.884 (back) 0.884 (mean)
$C_{Zn,low}$	0.948	0.888
$C_{Zn,scat}$	0.985	0.975
$C_{Au,scat}$	0.985 (front) 0.983 (back) 0.984 (mean)	0.981 (front) 0.979 (back) 0.980 (mean)
$C_{Zn,attn}$	1.015	1.016
$C_{Au,attn}$	1.019 (front) 1.010 (back) 1.01 (mean)	1.020 (front) 1.010 (back) 1.015 (mean)

3.3.1. Neutron flux fluctuation correction factor:

The effect of the fluctuation of neutron flux due to proton current fluctuation during the irradiation was taken into consideration. Its correction factor was obtained by

$$C_{x,fluc}=<\Phi_m>[1 - \exp(-\lambda_x t_1)] / [\Sigma_{i=1,n} \Phi_{m,i} [1 - \exp(-\lambda_x \Delta t_1)]\exp [-\lambda_x(t_1 - i\Delta t_1)]], \quad (12)$$

where $\Phi_{m,i}$ is the neutron flux measured by the NE213 monitor detector during the i-th time interval (i=1,n), $\Delta t_1=t_1/n$ (i.e., 30 min) and $<\Phi_m> =\Sigma_{i=1,n} \Phi_{m,i} / n$ [20,21].

3.3.2. Low energy background neutron correction factor:

The (p,n_1) low energy neutron background was subtracted by the correction factor

$$C_{x,low} = 1 - \int\varphi_1(E)\, \sigma_x(E)\, dE / \int\varphi(E)\, \sigma_x(E)\, dE, \quad (13)$$

where φ_1 (E) is the (p,n_1) neutron flux energy spectrum calculated by EPEN ($\varphi(E)=\varphi_0(E)+\varphi_1(E)$), and $\sigma_x(E)$ is the $^{70}Zn(n,\gamma)^{71}Zn^m$ cross section taken from the TENDL-2015 library [5] or $^{197}Au(n,\gamma)^{198}Au$ cross section taken from the IAEA Neutron Cross-Sections Standards [18].

3.3.3. Scattered neutron background correction factor:

Correction factors for the scattered neutron background C_{scat} originating from elastic, inelastic and multiple scattering in the foil stack and surrounding materials were evaluated by PHITS (Particle and Heavy Ion Transport code System) Ver 2.840 [22]. The experimental setup with all materials in and around the foil stack placed downstream of the tantalum proton beam stopper in Fig.3 was modelled in the simulation. Neutrons were generated according to the (p,n_0) neutron flux energy spectra $\varphi_0(E)$ calculated by EPEN and in the forward direction. Productions of ^{71m}Zn and ^{198}Au were calculated with the (p,n_0) neutron spectra from EPEN and evaluated cross sections of all foil stack and surrounding materials from the AceLibJ40 library (a library in the ACE

Format based on JENDL-4.0). Cross sections were calculated by counting ^{71m}Zn and ^{198}Au produced by all neutrons including neutrons scattered by a foil stack or surrounding material before the production (All), and those produced by neutrons not scattered before the production (True). The calculated cross sections and correction factors are summarized in **Table 11**. The uncertainties in C_{scat} are about 0.5% and 0.1% for Zn and Au foils, respectively. The weighted means of C_{scat} are adopted in determination of experimental cross sections because we cannot distinguish γ-rays from front and back foils in our measurement.

Table 11: Cross sections (mb) and correction factors calculated by PHITS with neutron flux energy spectra from EPEN and evaluated cross sections of all foil stack and surrounding materials in JENDL-4.0. The uncertainties in cross sections are standard deviations due to statistics from 500 M (Zn) and 100 M neutrons (Au).

E_n (MeV)	Foil	All	True	C_{scat}	(mean)
0.96	Au front	82.600 ± 0.076	81.350 ±0.068	0.985±0.001	0.984±0.001
	Au back	82.330 ± 0.073	80.940 ±0.068	0.983±0.001	
	Zn	1.378 ± 0.004	1.358 ±0.004	0.985±0.004	
1.69	Au front	70.440 ± 0.073	69.120 ±0.067	0.981±0.001	0.980±0.001
	Au back	66.750 ± 0.070	65.320 ±0.063	0.979±0.001	
	Zn	0.627 ± 0.003	0.611 ±0.002	0.975±0.005	

3.3.4 γ-ray self-attenuation factors:

Gamma spectrometric analysis requires correction for the self-attenuation effect due to the interactions of the γ-rays with the foil stack. Beer-Lambert's Law gives the probability to find a photon penetrating a distance x in a material (volume mass density ρ) as $\exp(-\mu_m \rho x)$ where μ_m is the mass attenuation coefficient of the γ energy and material. If the 1st foil (thickness x_1) is a

homogeneous source of the γ-line, and it penetrates other n-1 foils (thickness x_i) before reaching the detector, the probability of the penetration is expressed by [23-25]

$$C_{attn}^{-1} = [(1/x_1)\int_0^{x1} \exp(-\mu_{m,1}\rho_1 x)\, dx] \cdot \Pi_{i=2,n} \exp(-\mu_{m,i}\rho_i x_i)$$

$$= [[1- \exp(-\mu_{m,1}\rho_1 x_1)] /(\mu_{m,1}\rho_1 x_1)] \cdot \Pi_{i=2,n} \exp(-\mu_{m,i}\rho_i x_i) \qquad (14).$$

Table 12 shows the calculated self-attenuation factors of $^{71}Zn^m$ 386.28 keV and ^{198}Au 411.802 keV γ-rays penetrating the foil stack and detected by the detector behind the aluminium foil with the mass attenuation coefficients calculated by XMuDat Ver 1.01 [26].

Table 12: Self-attenuations factor at each medium of the foil stack calculated by XMuDat Ver 1.01 [26].

E_n (MeV)	Sample	^{198}Au E_γ = 411.802 keV	$^{71}Zn^m$ E_γ = 386.28 keV
0.96	Au (front)	0.9851	
	Zn	0.9969	0.9916
	Au (back)	0.9859	0.9840
	In	0.9957	0.9957
	Al	0.9994	0.9994
1.69	Au (front)	0.9847	
	Zn	0.9961	0.9915
	Au (back)	0.9855	0.9836
	In	0.9945	0.9945
	Al	0.9994	0.9994

4. NUCLEAR MODELS:

The excitation function of the $^{70}Zn(n,\gamma)^{71}Zn^{m}$reaction from 0.4 MeV to 4 MeV have been calculated using the nuclear reaction model code TALYS-1.6 [27] which was then compared with the measured cross sections. The optical model parameters for neutrons were obtained by a local potential proposed by Koning and Delaroche [28]. The compound nucleus contribution was calculated by the Hauser-Feshbach model [29]. The following five level density models available in TALYS-1.6 [27] were used:

- ldmodel1: the constant temperature and Fermi-gas model, where the constant temperature model is used in the low excitation region and the Fermi-gas model is used in the high excitation energy region. The transition energy is around the neutron separation energy.
- ldmodel2: the back-shifted Fermi-gas model.
- ldmodel3: the generalized superfluid model.
- ldmodel4: the microscopic level densities from Goriely's table [30].
- ldmodel5: the microscopic level densities from Hilaire's table [30].

The theoretical calculations have been done using the default parameter values except for the level density models.

5. RESULTS AND DISCUSSION:

The measured $^{70}Zn(n,\gamma)^{71}Zn^{m}$ cross sections are given in **Table 13** with their overall and partial uncertainties in **Table 14**. In Table 13, the ratio of the evaluated $^{70}Zn(n,\gamma)^{71}Zn^{m}$ cross sections in the TENDL-2015 library folded by the (p,n_0) neutron flux energy spectra $<\sigma_{Zn}^{m}>_{TENDL}$ to the measured cross sections are also given. Among the latest major libraries, JENDL-4.0 also provides an original evaluated data set for the $^{70}Zn(n,\gamma)^{71}Zn^{g+m}$ cross section [8] but not for the $^{70}Zn(n,\gamma)^{71}Zn^{m}$ cross section.

Fig. 7 shows the comparison of the present measured spectrum averaged cross sections with the cross sections for mono energetic neutrons predicted by TALYS-1.6 with various level density models. Sudden decrease of the $^{70}Zn(n,n_1)^{70}Zn^{m}$ cross section is predicted by both TALYS-1.6 and TENDL-2015 around 0.9 MeV. This is due to the $^{70}Zn(n,n_1)^{70}Zn$ inelastic scattering channel. It is clearly seen that the prediction with ldmodel3 (generalized superfluid model) agrees very well with the measured cross sections, while, the predictions with the all other level density models overestimate the measured cross sections.

In order to estimate the $^{70}Zn(n,\gamma)^{71}Zn^{g+m}$ cross sections from the measured $^{70}Zn(n,\gamma)^{71}Zn^{m}$ cross sections, the measured cross sections $<\sigma_{Zn}^{m}>_{exp}$ were multiplied by the isomeric ratios $<\sigma_{Zn}^{g+m}>_{TENDL}/<\sigma_{Zn}^{m}>_{TENDL}$ evaluated in TENDL-2015 folded by the $^{7}Li(p,n_0)$ neutron spectra (**Table 15**). **Table 16** compares the derived total neutron capture cross sections $<\sigma_{Zn}^{g+m}>_{present}$ with the (p,n_0) neutron flux energy spectrum averaged $^{70}Zn(n,\gamma)^{71}Zn^{g+m}$ cross sections evaluated in TENDL-2015 $<\sigma_{Zn}^{g+m}>_{TENDL}$, JENDL-4.0 $<\sigma_{Zn}^{g+m}>_{JENDL}$ as well as calculated by TALYS-1.6 with the generalized superfluid level density model (ldmodel3) $<\sigma_{Zn}^{g+m}>_{TALYS}$.

Table 13: The $^{70}Zn(n,\gamma)^{71}Zn^{m}$ cross sections measured in the present experiment $<\sigma_{Zn}^{m}>_{exp}$ with their total uncertainties. The ratio of the evaluated cross sections in TENDL-2015 averaged by the (p,n_0) neutron flux energy spectra $<\sigma_{Zn}^{m}>_{TENDL}$ to the measured cross sections are also given.

E_n (MeV)	$<\sigma_{Zn}^{m}>_{exp}$ (mb)	Correlation coefficients		$<\sigma_{Zn}^{m}>_{TENDL}/<\sigma_{Zn}^{m}>_{exp}$
0.96±0.15	1.83± 0.16	1.00		1.89
1.69±0.15	1.33± 0.09	0.12	1.00	1.48

Table 14: The fractional (%) partial uncertainty in the measured cross sections propagated from various sources of uncertainties. The last column gives the property of the correlation between two data points for each source of the uncertainty. See Appendix B for the propagation of the uncertainties in the half-lives.

Source		E_n=0.96 MeV	E_n=1.69 MeV	Correlation property*
Count	Zn	7.809	5.988	Uncorrelated
	Au	3.247	2.471	
Sample	Zn enrichment	1.381		Fully correlated
	Zn thickness	0.115	0.088	Uncorrelated
	Au thickness	0.099	0.097	
Decay data	Zn intensity	2.298		Fully correlated
	Au intensity	0.063		
	Zn half-life	0.177	0.273	
	Au half-life	0.027	0.015	
Other	Efficiency ratio	0.257		Fully correlated
	Au standard	1.043	1.433	Partially correlated†
Total		8.94	7.17	Partially correlated‡

* Uncorrelated, fully correlated and partially correlated mean the correlation coefficient is 0, 1 or between them, respectively. See Ref.[31] for more details.

† Correlation coefficient is 0.07 (See Table 9).

‡Correlation coefficient is 0.12, which is obtained by $(1.381^2 + 2.298^2 + 0.063^2 + 0.177\cdot0.273 + 0.027\cdot0.015 + 0.257^2 + 1.043\cdot1.433\cdot0.07) / (8.94\cdot7.17)$.

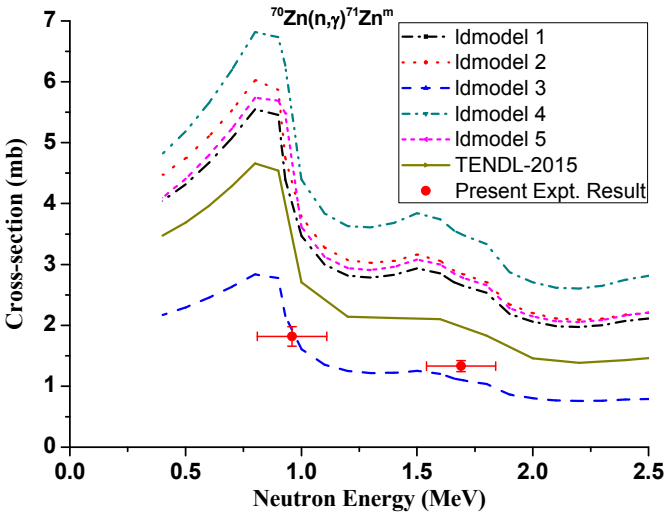

Fig. 7: Excitation functions of the ^{70}Zn(n,γ)^{71}Zn^{m} cross sections measured in this work, evaluated in TENDL-2015 (solid line) as well as calculated by TALYS-1.6 with five level density models. See text for the details of the level density models. The experimental cross sections are (p,n_0) neutron flux energy spectrum averaged while the evaluated and calculated cross sections are for mono energetic neutrons.

Table 15: The ^{70}Zn(n,γ)^{71}Zn^{m} and ^{70}Zn(n,γ)^{71}Zn^{g+m} cross sections folded by the (p,n_0) neutron flux energy spectra as well as their ratios in TENDL-2015.

E_n (MeV)	$\langle\sigma_{Zn}^{m}\rangle_{TENDL}$	$\langle\sigma_{Zn}^{g+m}\rangle_{TENDL}$	$\langle\sigma_{Zn}^{g+m}\rangle_{TENDL}$ /$\langle\sigma_{Zn}^{m}\rangle_{TENDL}$
0.96±0.15	3.4567	5.7720	1.6698
1.69±0.15	1.9689	3.3122	1.6823

Table 16: The $^{70}Zn(n,\gamma)^{71}Zn^{g+m}$ capture cross sections derived from the experimental $^{70}Zn(n,\gamma)^{71}Zn^{m}$ cross sections $<\sigma_{Zn}^{g+m}>_{present}$. The ratio of the evaluated cross sections folded by the (p,n_0) neutron flux energy spectra for TENDL-2015 $<\sigma_{Zn}^{g+m}>_{TENDL}$, JENDL-4.0 $<\sigma_{Zn}^{g+m}>_{JENDL}$, TALYS-1.6 with generalized superfluid level density model $<\sigma_{Zn}^{g+m}>_{TALYS}$ to the present cross sections are also given.

E_n (MeV)	$<\sigma_{Zn}^{g+m}>_{present}$ (mb)	$<\sigma_{Zn}^{g+m}>_{TENDL}/<\sigma_{Zn}^{g+m}>_{present}$	$<\sigma_{Zn}^{g+m}>_{JENDL}/<\sigma_{Zn}^{g+m}>_{present}$	$<\sigma_{Zn}^{g+m}>_{TALYS}/<\sigma_{Zn}^{g+m}>_{present}$
0.96±0.15	3.05 ± 0.27	1.90	1.15	1.33
1.69±0.15	2.24 ± 0.16	1.48	0.66	1.46

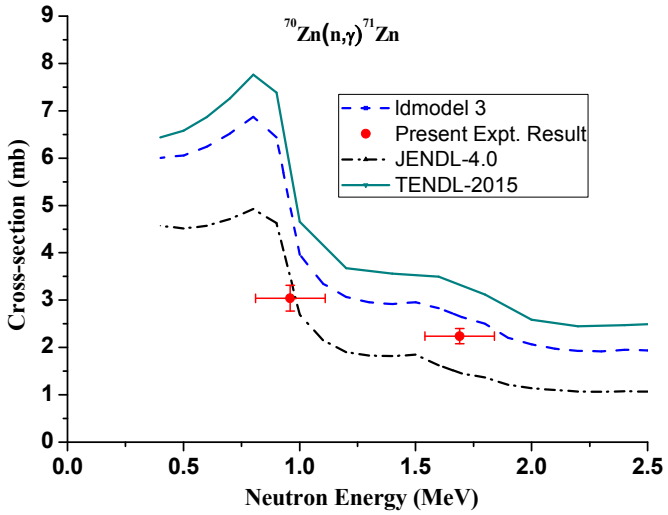

Fig. 8: Excitation functions of the $^{70}Zn(n,\gamma)^{71}Zn^{g+m}$ cross sections derived in the present work , evaluated in TENDL-2015 and JENDL-4.0 as well as calculated by TALYS-1.6 with the generalized superfluid level density model (ldmodel3). The derived present cross sections are (p,n_0) neutron flux energy spectrum averaged while the evaluated and calculated cross sections are for mono energetic neutrons.

Fig. 8 shows the excitation function for the $^{70}Zn(n,\gamma)^{71}Zn^{g+m}$ cross sections. It can be seen in this figure that the measured cross section is close to the JENDL-4.0 library at 0.96 MeV whereas between TENDL-2015 and JENDL-4.0 libraries at 1.69 MeV.

6. SUMMARIES AND CONCLUSION:

The $^{70}Zn(n,\gamma)^{71}Zn^{m}$ cross sections have been newly measured by a $^{7}Li(p,n)^{7}Be$ neutron source at 0.96 and 1.69 MeV, and their corresponding $^{70}Zn(n,\gamma)^{71}Zn^{m+g}$ cross sections have been derived. The data analysis is carried out using the latest decay data, and by taking into account the neutron flux fluctuation, low energy (p,n_1) neutron backgrounds, scattered neutron background, and γ self-attenuation. The measured $^{70}Zn(n,\gamma)^{71}Zn^{m}$ cross sections have been compared with theoretical calculations using TALYS-1.6 with various level density models. It has been observed that the theoretical calculation with default parameter settings and the generalized superfluid models predicts well the measured $^{70}Zn(n,\gamma)^{71}Zn^{m}$ cross sections whereas they are highly overestimated by calculations with all other level density models. The derived $^{70}Zn(n,\gamma)^{71}Zn^{g+m}$ cross sections have also been compared with the latest evaluated cross sections in the TENDL-2015 and JENDL-4.0 libraries. It has been observed that the present derived total cross section agrees well with the JENDL-4.0 library at 0.96 MeV whereas between TENDL-2015 and JENDL-4.0 libraries at 1.69 MeV.

ACKNOWLEDGMENTS

This work was carried out as a joint collaborative research project between the Department of Physics, Mizoram University and BARC, Mumbai under the financial support provided by the B.R.N.S., DAE, Mumbai. This work was also supported by the IAEA Nuclear Data Section. The authors are grateful to the TIFR, Mumbai for providing lithium target. The authors also gratefully

acknowledge the excellent cooperation of the FOTIA accelerator operators for smooth operation of the machine throughout the whole experiment. Dr. Valentina Semkova (IAEA Nuclear Data Section) provided us valuable comments on coincidence summing effects, and they are appreciated.

REFERENCES:

1. R. Reifarth, S. Dababneh, M. Heil, F. KÕppeler, R. Plag, K. Sonnabend, E. Uberseder, Phys. Rev. C **85** (2012) 035802.

2. Z. Bao, H. Beer, F. Käppeler, F. Voss, K. Wisshak, T. Rauscher, At. Data Nucl. Data Tables, **76** (2000) 70.

3. A. Trkov, Private communication (2015).

4. N. Otuka, E. Dupont, V. Semkova, B. Pritychenko, A.I. Blokhin, M. Aikawa, S. Babykina, M. Bossant, G. Chen, S. Dunaeva, R.A. Forrest, T. Fukahori, N. Furutachi, S. Ganesan, Z. Ge, O.O. Gritzay, M. Herman, S. Hlavač, K. Katō, B. Lalremruata, Y.O. Lee, A. Makinaga, K. Matsumoto, M. Mikhaylyukova, G. Pikulina, V.G. Pronyaev, A. Saxena, O. Schwerer, S.P. Simakov, N. Soppera, R. Suzuki, S. Takács, X. Tao, S. Taova, F. Tárkányi, V.V. Varlamov, J. Wang, S.C. Yang, V. Zerkin, Y. Zhuang, Nucl. Data Sheets **120** (2014) 272.

5. A.J. Koning, D. Rochman, J. Kopecky, J.Ch. Sublet, M. Fleming, E. Bauge, S. Hilaire, P. Romain, B. Morillon, H. Duarte, S.C van der Marck, S. Pomp, H. Sjostrand, R. Forresr, H. Henriksson, O. Cabellos, S. Goriely, J. Leppanen, H. Leeb, A. Plompen, R. Mills, "TENDL-2015: TALYS-based evaluated nuclear data library", [https://tendl.web.psi.ch/tendl_2015/tendl2015.html].

6. K. Shibata, O. Iwamoto, T. Nakagawa, N. Iwamoto, A. Ichihara, S. Kunieda, S. Chiba, K. Furutaka, N. Otuka, T. Ohsawa, T. Murata, H. Matsunobu, A. Zukeran, S. Kamada, J. Katakura, J. Nucl. Sci. Technol. **48** (2011) 1.

7. N. Iwamoto, J. Nucl. Sci. Technol. **44** (2007) 1131.

8. J.-Ch. Sublet, L.W. Packer, J. Kopecky, R.A. Forrest, A.J. Koning, D.A. Rochman, Report CCFE-R(1)05, Culham Centre for Fusion Energy, 2010.

9. R. Pachuau, B. Lalremruata, N. Otuka, L.R. Hlondo, L.R.M. Punte, H.H. Thanga, to be published in Nucl. Sci. Eng.; R. Pachuau, B. Lalremruata, N. Otuka, L.R. Hlondo, L.R.M. Punte, H.H. Thanga, to be published in the EPJ Web of Conferences (ND2016: International Conference on Nuclear Data for Science and Technology, 11 to 16 September 2016, Bruges, Belgium).

10. H. Liskien, A. Paulsen, At. Data Nucl. Data Tables **15** (1975) 57.

11. K. Abusaleem, B. Singh, Nucl. Data Sheets **112** (2011) 133.

12. Huang Xiaolong, Nucl. Data Sheets **110** (2009) 2533.

13. J. Blachot, Nucl. Data Sheets **113** (2012) 2391.

14. M.J. Martin, Nucl. Data Sheets **114** (2013) 1497.

15. R.W. Damon, "Determination of the photo-peak detection efficiency of a HpGe detector, for volume sources, via Monte Carlo simulations", Dissertation submitted to the University of the Western Cape, July 2005.

16. T. Vidmar, Nucl. Instrum. Meth. A **550** (2005) 603.

17. W. Mannhart, Report INDC(NDS)-0588 (Rev.), International Atomic Energy Agency, 2013.

18. A.D. Carlson, V.G. Pronyaev, D.L. Smith, N.M. Larson, Zhenpeng Chen, G.M. Hale, F.-J. Hambsch, E.V. Gai, Soo-Youl Oh, S.A. Badikov, T. Kawano, H.M. Hofmann, H. Vonach, S. Tagesen, Nucl. Data Sheets **110** (2009) 3215.

19. O. Bersillon, L.R. Greenwood, P.J. Griffin, W. Mannhart, H.J. Nolthenius, R. Paviotti-Corcuera, K.I. Zolotarev, E.M. Zsolnay, Report STI/DOC/010/452, International Atomic Energy Agency, 2006.

20. C. Sage, V. Semkova, O. Bouland, P. Dessagne, A. Fernandez, F. Gunsing, C. Nastren, G. Noguere, H. Ottmar, A.J.M. Plompen, P. Romain, G. Rudolf, J. Somers, F. Wastin, Phys. Rev. C **81** (2010) 064604.

21. A. Fessler, A.J.M. Plompen, D.L. Smith, J.W. Meadows, Y. Ikeda, Nucl. Sci. Eng. **134** (2000) 171.

22. T. Sato, K. Niita, N. Matsuda, S. Hashimoto, Y. Iwamoto, S. Noda, T. Ogawa, H. Iwase, H. Nakashima, T. Fukahori, K. Okumura, T. Kai, S. Chiba, T. Furuta, L. Sihver, J. Nucl. Sci. Technol. **50** (2013) 913.

23. D.W. Millsap, S. Landsberger, Appl. Radiat. Isot. **97** (2015) 21.

24. E. Robu, C. Giovani, Rom. Rep. Phys. **61** (2009) 295.

25. K.R. Jackman, "KMESS: An Open Source Software Package Using a Semi-empirical Mesh-Grid Method for the Modeling of Germanium Detector Efficiencies", Dissertation submitted to the University of Texas at Austin, August 2007.

26. R. Nowotny, Report IAEA-NDS-195, International Atomic Energy Agency, 1998.

27. A.J. Koning, D. Rochman, Nucl. Data Sheets **113** (2012) 2841.

28. A. J. Koning, J. P. Delaroche, Nucl. Phys. A **713** (2003) 231.

29. W. Hauser, H. Feshbach, Phys. Rev. **87** (1952) 366.

30. R. Capote, M. Herman, P. Oblozinsky, P.G. Young, S. Goriely, T. Belgya, A.V. Ignatyuk, A.J. Koning, S. Hilaire, V. Plujko, M. Avrigeanu, O. Bersillon, M.B. Chadwick, T. Fukahori, S. Kailas, J. Kopecky, V.M. Maslov, G. Reffo, M. Sin, E. Soukhovitskii, P. Talou, Han Yinlu, Ge Zhigang, Nucl. Data Sheets **110** (2009) 3107.

31. D.L. Smith, N Otuka, Nucl. Data Sheets **113** (2012) 3006.

APPENDIX A: The (p,n_0) and (p,n_1) neutron flux energy spectra $\varphi_0(E)$ and $\varphi_1(E)$ at proton energy 2.80 and 3.50 MeV.

E_p = 2.80±0.02 MeV			E_p = 3.50 ±0.02MeV		
E keV	$\varphi_0(E)$ neutrons/keV μC	$\varphi_1(E)$ neutrons/keV μC	E keV	$\varphi_0(E)$ neutrons/keV μC	$\varphi_1(E)$ neutrons/keV μC
231		1.0000E-03	995		0.0000E+00
232		1.0000E-03	996		0.0000E+00
233		3.0000E-03	997		0.0000E+00
234		5.0000E-03	998		0.0000E+00
235		5.0000E-03	999		0.0000E+00
236		9.0000E-03	1000		0.0000E+00
237		1.2000E-02	1001		0.0000E+00
238		1.8000E-02	1002		0.0000E+00
239		2.1000E-02	1003		0.0000E+00
240		3.2000E-02	1004		0.0000E+00
241		3.9000E-02	1005		0.0000E+00
242		5.3000E-02	1006		0.0000E+00
243		6.3000E-02	1007		0.0000E+00
244		8.7000E-02	1008		0.0000E+00
245		1.1800E-01	1009		0.0000E+00
246		1.3600E-01	1010		0.0000E+00
247		1.7200E-01	1011		0.0000E+00
248		2.0200E-01	1012		0.0000E+00
249		2.5000E-01	1013		0.0000E+00
250		2.8900E-01	1014		2.0000E-03
251		3.5300E-01	1015		2.0000E-03
252		4.2200E-01	1016		3.0000E-03
253		5.0200E-01	1017		3.0000E-03
254		5.7900E-01	1018		3.0000E-03
255		6.8200E-01	1019		6.0000E-03
256		7.9800E-01	1020		6.0000E-03
257		9.3400E-01	1021		8.0000E-03
258		1.0870E+00	1022		1.0000E-02
259		1.2610E+00	1023		1.2000E-02
260		1.4530E+00	1024		1.7000E-02
261		1.6820E+00	1025		2.0000E-02
262		1.9400E+00	1026		2.6000E-02
263		2.2330E+00	1027		3.1000E-02
264		2.5550E+00	1028		3.5000E-02
265		2.9250E+00	1029		4.7000E-02
266		3.3360E+00	1030		5.6000E-02
267		3.8030E+00	1031		6.9000E-02
268		4.3400E+00	1032		8.4000E-02
269		4.9330E+00	1033		1.0200E-01
270		5.6020E+00	1034		1.2300E-01
271		6.3570E+00	1035		1.4800E-01
272		7.2020E+00	1036		1.8100E-01
273		8.1500E+00	1037		2.1700E-01
274		9.2100E+00	1038		2.6100E-01
275		1.0395E+01	1039		3.1400E-01
276		1.1712E+01	1040		3.7600E-01
277		1.3181E+01	1041		4.4800E-01
278		1.4820E+01	1042		5.3400E-01
279		1.6632E+01	1043		6.3800E-01
280		1.8644E+01	1044		7.5700E-01

281	2.0869E+01	1045	8.9900E-01
282	2.3332E+01	1046	1.0640E+00
283	2.6049E+01	1047	1.2580E+00
284	2.9039E+01	1048	1.4820E+00
285	3.2338E+01	1049	1.7430E+00
286	3.5956E+01	1050	2.0450E+00
287	3.9931E+01	1051	2.3990E+00
288	4.4282E+01	1052	2.8080E+00
289	4.9045E+01	1053	3.2780E+00
290	5.4255E+01	1054	3.8220E+00
291	5.9933E+01	1055	4.4450E+00
292	6.6106E+01	1056	5.1590E+00
293	7.2837E+01	1057	5.9840E+00
294	8.0134E+01	1058	6.9250E+00
295	8.8045E+01	1059	8.0010E+00
296	9.6605E+01	1060	9.2190E+00
297	1.0588E+02	1061	1.0614E+01
298	1.1587E+02	1062	1.2186E+01
299	1.2664E+02	1063	1.3975E+01
300	1.3825E+02	1064	1.6003E+01
301	1.5068E+02	1065	1.8280E+01
302	1.6404E+02	1066	2.0851E+01
303	1.7835E+02	1067	2.3745E+01
304	1.9370E+02	1068	2.6998E+01
305	2.1007E+02	1069	3.0634E+01
306	2.2748E+02	1070	3.4698E+01
307	2.4605E+02	1071	3.9236E+01
308	2.6581E+02	1072	4.4304E+01
309	2.8682E+02	1073	4.9934E+01
310	3.0902E+02	1074	5.6178E+01
311	3.3253E+02	1075	6.3113E+01
312	3.5738E+02	1076	7.0783E+01
313	3.8360E+02	1077	7.9244E+01
314	4.1127E+02	1078	8.8572E+01
315	4.4037E+02	1079	9.8872E+01
316	4.7093E+02	1080	1.1014E+02
317	5.0290E+02	1081	1.2253E+02
318	5.3645E+02	1082	1.3610E+02
319	5.7155E+02	1083	1.5093E+02
320	6.0820E+02	1084	1.6705E+02
321	6.4639E+02	1085	1.8468E+02
322	6.8607E+02	1086	2.0384E+02
323	7.2738E+02	1087	2.2464E+02
324	7.7022E+02	1088	2.4714E+02
325	8.1473E+02	1089	2.7155E+02
326	8.6075E+02	1090	2.9797E+02
327	9.0816E+02	1091	3.2634E+02
328	9.5703E+02	1092	3.5699E+02
329	1.0075E+03	1093	3.8979E+02
330	1.0595E+03	1094	4.2517E+02
331	1.1127E+03	1095	4.6292E+02
332	1.1673E+03	1096	5.0348E+02
333	1.2233E+03	1097	5.4673E+02
334	1.2804E+03	1098	5.9274E+02
335	1.3387E+03	1099	6.4174E+02
336	1.3981E+03	1100	6.9390E+02
337	1.4587E+03	1101	7.4930E+02
338	1.5202E+03	1102	8.0801E+02

339	1.5826E+03	1103	8.6991E+02
340	1.6458E+03	1104	9.3541E+02
341	1.7098E+03	1105	1.0046E+03
342	1.7744E+03	1106	1.0772E+03
343	1.8395E+03	1107	1.1538E+03
344	1.9051E+03	1108	1.2340E+03
345	1.9710E+03	1109	1.3183E+03
346	2.0373E+03	1110	1.4063E+03
347	2.1037E+03	1111	1.4983E+03
348	2.1702E+03	1112	1.5942E+03
349	2.2369E+03	1113	1.6945E+03
350	2.3032E+03	1114	1.7984E+03
351	2.3695E+03	1115	1.9062E+03
352	2.4355E+03	1116	2.0182E+03
353	2.5010E+03	1117	2.1345E+03
354	2.5660E+03	1118	2.2541E+03
355	2.6305E+03	1119	2.3783E+03
356	2.6944E+03	1120	2.5059E+03
357	2.7575E+03	1121	2.6374E+03
358	2.8200E+03	1122	2.7724E+03
359	2.8812E+03	1123	2.9110E+03
360	2.9418E+03	1124	3.0530E+03
361	3.0012E+03	1125	3.1984E+03
362	3.0597E+03	1126	3.3470E+03
363	3.1170E+03	1127	3.4986E+03
364	3.1730E+03	1128	3.6528E+03
365	3.2278E+03	1129	3.8098E+03
366	3.2813E+03	1130	3.9693E+03
367	3.3335E+03	1131	4.1313E+03
368	3.3845E+03	1132	4.2951E+03
369	3.4341E+03	1133	4.4608E+03
370	3.4822E+03	1134	4.6284E+03
371	3.5288E+03	1135	4.7967E+03
372	3.5740E+03	1136	4.9665E+03
373	3.6178E+03	1137	5.1375E+03
374	3.6603E+03	1138	5.3090E+03
375	3.7012E+03	1139	5.4804E+03
376	3.7410E+03	1140	5.6526E+03
377	3.7794E+03	1141	5.8243E+03
378	3.8162E+03	1142	5.9959E+03
379	3.8515E+03	1143	6.1667E+03
380	3.8857E+03	1144	6.3368E+03
381	3.9186E+03	1145	6.5057E+03
382	3.9502E+03	1146	6.6733E+03
383	3.9808E+03	1147	6.8392E+03
384	4.0100E+03	1148	7.0037E+03
385	4.0379E+03	1149	7.1654E+03
386	4.0649E+03	1150	7.3253E+03
387	4.0907E+03	1151	7.4825E+03
388	4.1155E+03	1152	7.6373E+03
389	4.1397E+03	1153	7.7888E+03
390	4.1628E+03	1154	7.9374E+03
391	4.1853E+03	1155	8.0829E+03
392	4.2065E+03	1156	8.2251E+03
393	4.2274E+03	1157	8.3635E+03
394	4.2474E+03	1158	8.4983E+03
395	4.2667E+03	1159	8.6297E+03
396	4.2854E+03	1160	8.7571E+03

397	4.3036E+03	1161	8.8803E+03
398	4.3212E+03	1162	8.9999E+03
399	4.3381E+03	1163	9.1154E+03
400	4.3547E+03	1164	9.2267E+03
401	4.3709E+03	1165	9.3340E+03
402	4.3866E+03	1166	9.4373E+03
403	4.4018E+03	1167	9.5361E+03
404	4.4167E+03	1168	9.6308E+03
405	4.4313E+03	1169	9.7220E+03
406	4.4455E+03	1170	9.8085E+03
407	4.4596E+03	1171	9.8911E+03
408	4.4732E+03	1172	9.9700E+03
409	4.4869E+03	1173	1.0045E+04
410	4.5003E+03	1174	1.0116E+04
411	4.5132E+03	1175	1.0183E+04
412	4.5261E+03	1176	1.0247E+04
413	4.5388E+03	1177	1.0307E+04
414	4.5512E+03	1178	1.0364E+04
415	4.5638E+03	1179	1.0418E+04
416	4.5761E+03	1180	1.0469E+04
417	4.5886E+03	1181	1.0516E+04
418	4.6006E+03	1182	1.0561E+04
419	4.6129E+03	1183	1.0603E+04
420	4.6246E+03	1184	1.0641E+04
421	4.6366E+03	1185	1.0678E+04
422	4.6483E+03	1186	1.0712E+04
423	4.6602E+03	1187	1.0744E+04
424	4.6720E+03	1188	1.0773E+04
425	4.6840E+03	1189	1.0801E+04
426	4.6955E+03	1190	1.0827E+04
427	4.7073E+03	1191	1.0850E+04
428	4.7189E+03	1192	1.0872E+04
429	4.7304E+03	1193	1.0893E+04
430	4.7418E+03	1194	1.0912E+04
431	4.7536E+03	1195	1.0929E+04
432	4.7652E+03	1196	1.0946E+04
433	4.7769E+03	1197	1.0961E+04
434	4.7885E+03	1198	1.0975E+04
435	4.8001E+03	1199	1.0988E+04
436	4.8116E+03	1200	1.1000E+04
437	4.8231E+03	1201	1.1012E+04
438	4.8345E+03	1202	1.1022E+04
439	4.8462E+03	1203	1.1032E+04
440	4.8577E+03	1204	1.1041E+04
441	4.8695E+03	1205	1.1050E+04
442	4.8812E+03	1206	1.1058E+04
443	4.8927E+03	1207	1.1065E+04
444	4.9043E+03	1208	1.1072E+04
445	4.9160E+03	1209	1.1079E+04
446	4.9274E+03	1210	1.1085E+04
447	4.9390E+03	1211	1.1091E+04
448	4.9507E+03	1212	1.1097E+04
449	4.9623E+03	1213	1.1102E+04
450	4.9742E+03	1214	1.1108E+04
451	4.9856E+03	1215	1.1112E+04
452	4.9974E+03	1216	1.1117E+04
453	5.0090E+03	1217	1.1122E+04
454	5.0209E+03	1218	1.1126E+04

455	5.0326E+03	1219	1.1130E+04
456	5.0441E+03	1220	1.1135E+04
457	5.0558E+03	1221	1.1139E+04
458	5.0676E+03	1222	1.1143E+04
459	5.0792E+03	1223	1.1147E+04
460	5.0909E+03	1224	1.1151E+04
461	5.1027E+03	1225	1.1154E+04
462	5.1146E+03	1226	1.1158E+04
463	5.1265E+03	1227	1.1162E+04
464	5.1382E+03	1228	1.1166E+04
465	5.1497E+03	1229	1.1170E+04
466	5.1618E+03	1230	1.1173E+04
467	5.1733E+03	1231	1.1177E+04
468	5.1850E+03	1232	1.1180E+04
469	5.1968E+03	1233	1.1184E+04
470	5.2086E+03	1234	1.1187E+04
471	5.2205E+03	1235	1.1191E+04
472	5.2322E+03	1236	1.1194E+04
473	5.2441E+03	1237	1.1197E+04
474	5.2560E+03	1238	1.1201E+04
475	5.2673E+03	1239	1.1204E+04
476	5.2790E+03	1240	1.1207E+04
477	5.2906E+03	1241	1.1210E+04
478	5.3023E+03	1242	1.1213E+04
479	5.3141E+03	1243	1.1216E+04
480	5.3257E+03	1244	1.1219E+04
481	5.3373E+03	1245	1.1222E+04
482	5.3489E+03	1246	1.1224E+04
483	5.3606E+03	1247	1.1227E+04
484	5.3719E+03	1248	1.1229E+04
485	5.3830E+03	1249	1.1231E+04
486	5.3945E+03	1250	1.1233E+04
487	5.4059E+03	1251	1.1235E+04
488	5.4171E+03	1252	1.1237E+04
489	5.4286E+03	1253	1.1238E+04
490	5.4398E+03	1254	1.1239E+04
491	5.4511E+03	1255	1.1240E+04
492	5.4623E+03	1256	1.1241E+04
493	5.4736E+03	1257	1.1241E+04
494	5.4846E+03	1258	1.1241E+04
495	5.4955E+03	1259	1.1240E+04
496	5.5064E+03	1260	1.1239E+04
497	5.5175E+03	1261	1.1237E+04
498	5.5285E+03	1262	1.1235E+04
499	5.5396E+03	1263	1.1232E+04
500	5.5505E+03	1264	1.1229E+04
501	5.5613E+03	1265	1.1224E+04
502	5.5722E+03	1266	1.1219E+04
503	5.5831E+03	1267	1.1213E+04
504	5.5940E+03	1268	1.1206E+04
505	5.6046E+03	1269	1.1198E+04
506	5.6155E+03	1270	1.1189E+04
507	5.6264E+03	1271	1.1179E+04
508	5.6373E+03	1272	1.1168E+04
509	5.6480E+03	1273	1.1155E+04
510	5.6588E+03	1274	1.1141E+04
511	5.6696E+03	1275	1.1125E+04
512	5.6805E+03	1276	1.1108E+04

513	5.6914E+03	1277	1.1089E+04
514	5.7020E+03	1278	1.1068E+04
515	5.7127E+03	1279	1.1046E+04
516	5.7232E+03	1280	1.1021E+04
517	5.7339E+03	1281	1.0993E+04
518	5.7443E+03	1282	1.0964E+04
519	5.7548E+03	1283	1.0933E+04
520	5.7652E+03	1284	1.0899E+04
521	5.7755E+03	1285	1.0862E+04
522	5.7858E+03	1286	1.0823E+04
523	5.7960E+03	1287	1.0781E+04
524	5.8060E+03	1288	1.0736E+04
525	5.8160E+03	1289	1.0688E+04
526	5.8256E+03	1290	1.0638E+04
527	5.8348E+03	1291	1.0584E+04
528	5.8442E+03	1292	1.0526E+04
529	5.8531E+03	1293	1.0465E+04
530	5.8620E+03	1294	1.0401E+04
531	5.8706E+03	1295	1.0333E+04
532	5.8789E+03	1296	1.0262E+04
533	5.8870E+03	1297	1.0187E+04
534	5.8944E+03	1298	1.0108E+04
535	5.9018E+03	1299	1.0024E+04
536	5.9084E+03	1300	9.9380E+03
537	5.9147E+03	1301	9.8471E+03
538	5.9200E+03	1302	9.7525E+03
539	5.9250E+03	1303	9.6542E+03
540	5.9295E+03	1304	9.5515E+03
541	5.9332E+03	1305	9.4447E+03
542	5.9363E+03	1306	9.3341E+03
543	5.9387E+03	1307	9.2197E+03
544	5.9400E+03	1308	9.1010E+03
545	5.9405E+03	1309	8.9780E+03
546	5.9399E+03	1310	8.8524E+03
547	5.9386E+03	1311	8.7221E+03
548	5.9354E+03	1312	8.5884E+03
549	5.9314E+03	1313	8.4509E+03
550	5.9261E+03	1314	8.3104E+03
551	5.9193E+03	1315	8.1664E+03
552	5.9113E+03	1316	8.0188E+03
553	5.9015E+03	1317	7.8681E+03
554	5.8904E+03	1318	7.7149E+03
555	5.8772E+03	1319	7.5584E+03
556	5.8628E+03	1320	7.3997E+03
557	5.8459E+03	1321	7.2385E+03
558	5.8275E+03	1322	7.0747E+03
559	5.8065E+03	1323	6.9089E+03
560	5.7836E+03	1324	6.7413E+03
561	5.7586E+03	1325	6.5723E+03
562	5.7311E+03	1326	6.4022E+03
563	5.7016E+03	1327	6.2301E+03
564	5.6696E+03	1328	6.0576E+03
565	5.6348E+03	1329	5.8843E+03
566	5.5977E+03	1330	5.7105E+03
567	5.5579E+03	1331	5.5365E+03
568	5.5155E+03	1332	5.3627E+03
569	5.4701E+03	1333	5.1889E+03
570	5.4222E+03	1334	5.0157E+03

571	5.3710E+03	1335	4.8432E+03
572	5.3176E+03	1336	4.6722E+03
573	5.2611E+03	1337	4.5019E+03
574	5.2017E+03	1338	4.3330E+03
575	5.1395E+03	1339	4.1662E+03
576	5.0745E+03	1340	4.0013E+03
577	5.0070E+03	1341	3.8386E+03
578	4.9361E+03	1342	3.6782E+03
579	4.8629E+03	1343	3.5206E+03
580	4.7868E+03	1344	3.3652E+03
581	4.7084E+03	1345	3.2132E+03
582	4.6271E+03	1346	3.0643E+03
583	4.5437E+03	1347	2.9186E+03
584	4.4576E+03	1348	2.7764E+03
585	4.3692E+03	1349	2.6376E+03
586	4.2790E+03	1350	2.5029E+03
587	4.1867E+03	1351	2.3715E+03
588	4.0924E+03	1352	2.2441E+03
589	3.9963E+03	1353	2.1207E+03
590	3.8988E+03	1354	2.0014E+03
591	3.7999E+03	1355	1.8861E+03
592	3.6997E+03	1356	1.7751E+03
593	3.5985E+03	1357	1.6682E+03
594	3.4963E+03	1358	1.5657E+03
595	3.3933E+03	1359	1.4672E+03
596	3.2899E+03	1360	1.3729E+03
597	3.1859E+03	1361	1.2828E+03
598	3.0820E+03	1362	1.1969E+03
599	2.9776E+03	1363	1.1149E+03
600	2.8741E+03	1364	1.0371E+03
601	2.7705E+03	1365	9.6323E+02
602	2.6679E+03	1366	8.9320E+02
603	2.5656E+03	1367	8.2704E+02
604	2.4644E+03	1368	7.6450E+02
605	2.3643E+03	1369	7.0550E+02
606	2.2655E+03	1370	6.5015E+02
607	2.1679E+03	1371	5.9798E+02
608	2.0720E+03	1372	5.4939E+02
609	1.9778E+03	1373	5.0374E+02
610	1.8853E+03	1374	4.6105E+02
611	1.7951E+03	1375	4.2134E+02
612	1.7065E+03	1376	3.8440E+02
613	1.6204E+03	1377	3.5012E+02
614	1.5365E+03	1378	3.1836E+02
615	1.4551E+03	1379	2.8893E+02
616	1.3759E+03	1380	2.6176E+02
617	1.2993E+03	1381	2.3678E+02
618	1.2253E+03	1382	2.1380E+02
619	1.1538E+03	1383	1.9270E+02
620	1.0850E+03	1384	1.7336E+02
621	1.0188E+03	1385	1.5570E+02
622	9.5521E+02	1386	1.3955E+02
623	8.9435E+02	1387	1.2486E+02
624	8.3609E+02	1388	1.1152E+02
625	7.8045E+02	1389	9.9426E+01
626	7.2744E+02	1390	8.8462E+01
627	6.7709E+02	1391	7.8582E+01
628	6.2925E+02	1392	6.9678E+01

629	5.8396E+02	1393	6.1650E+01
630	5.4102E+02	1394	5.4432E+01
631	5.0047E+02	1395	4.7989E+01
632	4.6217E+02	1396	4.2228E+01
633	4.2622E+02	1397	3.7078E+01
634	3.9238E+02	1398	3.2502E+01
635	3.6076E+02	1399	2.8432E+01
636	3.3110E+02	1400	2.4823E+01
637	3.0340E+02	1401	2.1627E+01
638	2.7757E+02	1402	1.8811E+01
639	2.5356E+02	1403	1.6328E+01
640	2.3122E+02	1404	1.4142E+01
641	2.1050E+02	1405	1.2226E+01
642	1.9136E+02	1406	1.0547E+01
643	1.7362E+02	1407	9.0800E+00
644	1.5730E+02	1408	7.8030E+00
645	1.4228E+02	1409	6.6950E+00
646	1.2846E+02	1410	5.7290E+00
647	1.1579E+02	1411	4.8930E+00
648	1.0422E+02	1412	4.1730E+00
649	9.3601E+01	1413	3.5470E+00
650	8.3964E+01	1414	3.0140E+00
651	7.5160E+01	1415	2.5530E+00
652	6.7190E+01	1416	2.1570E+00
653	5.9947E+01	1417	1.8230E+00
654	5.3392E+01	1418	1.5330E+00
655	4.7478E+01	1419	1.2910E+00
656	4.2141E+01	1420	1.0800E+00
657	3.7334E+01	1421	9.0200E-01
658	3.3019E+01	1422	7.5600E-01
659	2.9156E+01	1423	6.2900E-01
660	2.5697E+01	1424	5.2300E-01
661	2.2609E+01	1425	4.3200E-01
662	1.9854E+01	1426	3.5900E-01
663	1.7406E+01	1427	2.9800E-01
664	1.5232E+01	1428	2.4600E-01
665	1.3306E+01	1429	2.0100E-01
666	1.1602E+01	1430	1.6500E-01
667	1.0097E+01	1431	1.3700E-01
668	8.7770E+00	1432	1.1100E-01
669	7.6060E+00	1433	9.0000E-02
670	6.5860E+00	1434	7.1000E-02
671	5.6880E+00	1435	6.0000E-02
672	4.9080E+00	1436	4.6000E-02
673	4.2260E+00	1437	3.8000E-02
674	3.6290E+00	1438	3.1000E-02
675	3.1140E+00	1439	2.4000E-02
676	2.6650E+00	1440	2.1000E-02
677	2.2770E+00	1441	1.5000E-02
678	1.9420E+00	1442	1.4000E-02
679	1.6540E+00	1443	9.0000E-03
680	1.4020E+00	1444	8.0000E-03
681	1.1900E+00	1445	7.0000E-03
682	1.0100E+00	1446	5.0000E-03
683	8.5100E-01	1447	4.0000E-03
684	7.1700E-01	1448	0.0000E+00
685	6.0400E-01	1449	0.0000E+00
686	5.0800E-01	1450	0.0000E+00

687		4.2700E-01	1451	0.0000E+00
688		3.5500E-01	1452	0.0000E+00
689		2.9900E-01	1453	0.0000E+00
690		2.4700E-01	1454	0.0000E+00
691		2.0700E-01	1455	0.0000E+00
692		1.6900E-01	1456	0.0000E+00
693		1.4100E-01	1457	0.0000E+00
694		1.1700E-01	1458	0.0000E+00
695		9.7000E-02	1459	0.0000E+00
696		8.0000E-02	1460	0.0000E+00
697		6.6000E-02	1461	0.0000E+00
698		5.3000E-02	1462	0.0000E+00
699		4.2000E-02	1463	0.0000E+00
700		3.7000E-02	1464	1.0000E-03
701		2.9000E-02	1465	2.0000E-03
702		2.3000E-02	1466	2.0000E-03
703		2.0000E-02	1467	2.0000E-03
704		1.5000E-02	1468	4.0000E-03
705		1.1000E-02	1469	4.0000E-03
706		1.0000E-02	1470	6.0000E-03
707		8.0000E-03	1471	7.0000E-03
708		7.0000E-03	1472	1.0000E-02
709		5.0000E-03	1473	1.2000E-02
710		0.0000E+00	1474	1.4000E-02
711		0.0000E+00	1475	1.9000E-02
712		0.0000E+00	1476	2.5000E-02
713	0.0000E+00		1477	3.0000E-02
714	0.0000E+00		1478	3.8000E-02
715	0.0000E+00		1479	4.9000E-02
716	0.0000E+00		1480	6.0000E-02
717	0.0000E+00		1481	7.6000E-02
718	0.0000E+00		1482	9.5000E-02
719	0.0000E+00		1483	1.1700E-01
720	0.0000E+00		1484	1.4600E-01
721	1.0000E-03		1485	1.8300E-01
722	3.0000E-03		1486	2.2300E-01
723	3.0000E-03		1487	2.7400E-01
724	4.0000E-03		1488	3.3800E-01
725	4.0000E-03		1489	4.1500E-01
726	7.0000E-03		1490	5.0600E-01
727	9.0000E-03		1491	6.1700E-01
728	1.2000E-02		1492	7.5300E-01
729	1.5000E-02		1493	9.1300E-01
730	2.0000E-02		1494	1.1070E+00
731	2.3000E-02		1495	1.3410E+00
732	3.0000E-02		1496	1.6190E+00
733	3.8000E-02		1497	1.9510E+00
734	4.7000E-02		1498	2.3450E+00
735	6.2000E-02		1499	2.8150E+00
736	7.6000E-02		1500	3.3690E+00
737	9.4000E-02		1501	4.0260E+00
738	1.1900E-01		1502	4.8040E+00
739	1.4700E-01		1503	5.7090E+00
740	1.8300E-01		1504	6.7820E+00
741	2.2700E-01		1505	8.0370E+00
742	2.8300E-01		1506	9.5080E+00
743	3.4700E-01		1507	1.1220E+01
744	4.3000E-01		1508	1.3219E+01

745	5.2600E-01	1509	1.5541E+01
746	6.4800E-01	1510	1.8242E+01
747	7.9300E-01	1511	2.1369E+01
748	9.7100E-01	1512	2.4960E+01
749	1.1840E+00	1513	2.9132E+01
750	1.4430E+00	1514	3.3915E+01
751	1.7540E+00	1515	3.9418E+01
752	2.1270E+00	1516	4.5710E+01
753	2.5750E+00	1517	5.2925E+01
754	3.1110E+00	1518	6.1143E+01
755	3.7520E+00	1519	7.0547E+01
756	4.5180E+00	1520	8.1226E+01
757	5.4250E+00	1521	9.3319E+01
758	6.5070E+00	1522	1.0707E+02
759	7.7830E+00	1523	1.2257E+02
760	9.2960E+00	1524	1.4013E+02
761	1.1083E+01	1525	1.5985E+02
762	1.3181E+01	1526	1.8201E+02
763	1.5645E+01	1527	2.0697E+02
764	1.8539E+01	1528	2.3485E+02
765	2.1930E+01	1529	2.6615E+02
766	2.5893E+01	1530	3.0099E+02
767	3.0495E+01	1531	3.3984E+02
768	3.5875E+01	1532	3.8297E+02
769	4.2093E+01	1533	4.3095E+02
770	4.9308E+01	1534	4.8399E+02
771	5.7670E+01	1535	5.4290E+02
772	6.7285E+01	1536	6.0783E+02
773	7.8374E+01	1537	6.7934E+02
774	9.1153E+01	1538	7.5816E+02
775	1.0580E+02	1539	8.4467E+02
776	1.2256E+02	1540	9.3968E+02
777	1.4174E+02	1541	1.0438E+03
778	1.6351E+02	1542	1.1576E+03
779	1.8834E+02	1543	1.2815E+03
780	2.1660E+02	1544	1.4167E+03
781	2.4860E+02	1545	1.5637E+03
782	2.8488E+02	1546	1.7237E+03
783	3.2579E+02	1547	1.8971E+03
784	3.7189E+02	1548	2.0844E+03
785	4.2379E+02	1549	2.2870E+03
786	4.8205E+02	1550	2.5054E+03
787	5.4728E+02	1551	2.7416E+03
788	6.2034E+02	1552	2.9952E+03
789	7.0183E+02	1553	3.2672E+03
790	7.9252E+02	1554	3.5590E+03
791	8.9376E+02	1555	3.8720E+03
792	1.0057E+03	1556	4.2069E+03
793	1.1301E+03	1557	4.5630E+03
794	1.2671E+03	1558	4.9437E+03
795	1.4188E+03	1559	5.3483E+03
796	1.5860E+03	1560	5.7783E+03
797	1.7699E+03	1561	6.2353E+03
798	1.9709E+03	1562	6.7189E+03
799	2.1919E+03	1563	7.2312E+03
800	2.4332E+03	1564	7.7703E+03
801	2.6964E+03	1565	8.3417E+03
802	2.9837E+03	1566	8.9429E+03

803	3.2954E+03	1567	9.5754E+03
804	3.6334E+03	1568	1.0238E+04
805	4.0006E+03	1569	1.0936E+04
806	4.3978E+03	1570	1.1664E+04
807	4.8260E+03	1571	1.2427E+04
808	5.2867E+03	1572	1.3224E+04
809	5.7819E+03	1573	1.4056E+04
810	6.3149E+03	1574	1.4921E+04
811	6.8851E+03	1575	1.5823E+04
812	7.4942E+03	1576	1.6757E+04
813	8.1454E+03	1577	1.7725E+04
814	8.8389E+03	1578	1.8731E+04
815	9.5767E+03	1579	1.9770E+04
816	1.0360E+04	1580	2.0841E+04
817	1.1191E+04	1581	2.1949E+04
818	1.2067E+04	1582	2.3091E+04
819	1.2996E+04	1583	2.4263E+04
820	1.3973E+04	1584	2.5467E+04
821	1.5001E+04	1585	2.6704E+04
822	1.6081E+04	1586	2.7970E+04
823	1.7213E+04	1587	2.9265E+04
824	1.8397E+04	1588	3.0590E+04
825	1.9635E+04	1589	3.1943E+04
826	2.0925E+04	1590	3.3318E+04
827	2.2267E+04	1591	3.4719E+04
828	2.3663E+04	1592	3.6144E+04
829	2.5112E+04	1593	3.7589E+04
830	2.6606E+04	1594	3.9054E+04
831	2.8156E+04	1595	4.0536E+04
832	2.9753E+04	1596	4.2035E+04
833	3.1396E+04	1597	4.3550E+04
834	3.3084E+04	1598	4.5078E+04
835	3.4819E+04	1599	4.6611E+04
836	3.6593E+04	1600	4.8156E+04
837	3.8409E+04	1601	4.9706E+04
838	4.0259E+04	1602	5.1261E+04
839	4.2144E+04	1603	5.2818E+04
840	4.4063E+04	1604	5.4375E+04
841	4.6010E+04	1605	5.5927E+04
842	4.7980E+04	1606	5.7479E+04
843	4.9973E+04	1607	5.9020E+04
844	5.1985E+04	1608	6.0556E+04
845	5.4014E+04	1609	6.2078E+04
846	5.6051E+04	1610	6.3588E+04
847	5.8098E+04	1611	6.5084E+04
848	6.0148E+04	1612	6.6564E+04
849	6.2199E+04	1613	6.8023E+04
850	6.4249E+04	1614	6.9461E+04
851	6.6289E+04	1615	7.0876E+04
852	6.8319E+04	1616	7.2271E+04
853	7.0332E+04	1617	7.3635E+04
854	7.2325E+04	1618	7.4972E+04
855	7.4297E+04	1619	7.6282E+04
856	7.6253E+04	1620	7.7562E+04
857	7.8168E+04	1621	7.8807E+04
858	8.0056E+04	1622	8.0021E+04
859	8.1910E+04	1623	8.1203E+04
860	8.3726E+04	1624	8.2348E+04

861	8.5506E+04	1625	8.3458E+04
862	8.7233E+04	1626	8.4531E+04
863	8.8927E+04	1627	8.5570E+04
864	9.0565E+04	1628	8.6569E+04
865	9.2158E+04	1629	8.7532E+04
866	9.3703E+04	1630	8.8458E+04
867	9.5189E+04	1631	8.9345E+04
868	9.6626E+04	1632	9.0195E+04
869	9.8014E+04	1633	9.1008E+04
870	9.9343E+04	1634	9.1783E+04
871	1.0062E+05	1635	9.2519E+04
872	1.0184E+05	1636	9.3223E+04
873	1.0300E+05	1637	9.3890E+04
874	1.0411E+05	1638	9.4519E+04
875	1.0516E+05	1639	9.5117E+04
876	1.0616E+05	1640	9.5682E+04
877	1.0710E+05	1641	9.6213E+04
878	1.0799E+05	1642	9.6710E+04
879	1.0883E+05	1643	9.7182E+04
880	1.0962E+05	1644	9.7620E+04
881	1.1035E+05	1645	9.8030E+04
882	1.1103E+05	1646	9.8411E+04
883	1.1167E+05	1647	9.8771E+04
884	1.1227E+05	1648	9.9102E+04
885	1.1282E+05	1649	9.9410E+04
886	1.1332E+05	1650	9.9694E+04
887	1.1379E+05	1651	9.9959E+04
888	1.1422E+05	1652	1.0020E+05
889	1.1461E+05	1653	1.0043E+05
890	1.1497E+05	1654	1.0063E+05
891	1.1529E+05	1655	1.0082E+05
892	1.1558E+05	1656	1.0099E+05
893	1.1584E+05	1657	1.0115E+05
894	1.1607E+05	1658	1.0129E+05
895	1.1628E+05	1659	1.0142E+05
896	1.1646E+05	1660	1.0154E+05
897	1.1661E+05	1661	1.0165E+05
898	1.1674E+05	1662	1.0174E+05
899	1.1685E+05	1663	1.0183E+05
900	1.1694E+05	1664	1.0191E+05
901	1.1700E+05	1665	1.0198E+05
902	1.1706E+05	1666	1.0204E+05
903	1.1709E+05	1667	1.0210E+05
904	1.1712E+05	1668	1.0215E+05
905	1.1713E+05	1669	1.0219E+05
906	1.1712E+05	1670	1.0223E+05
907	1.1711E+05	1671	1.0226E+05
908	1.1709E+05	1672	1.0230E+05
909	1.1706E+05	1673	1.0232E+05
910	1.1702E+05	1674	1.0235E+05
911	1.1697E+05	1675	1.0236E+05
912	1.1691E+05	1676	1.0238E+05
913	1.1685E+05	1677	1.0240E+05
914	1.1678E+05	1678	1.0241E+05
915	1.1671E+05	1679	1.0242E+05
916	1.1663E+05	1680	1.0243E+05
917	1.1655E+05	1681	1.0244E+05
918	1.1646E+05	1682	1.0244E+05

919	1.1638E+05	1683	1.0245E+05
920	1.1628E+05	1684	1.0246E+05
921	1.1619E+05	1685	1.0246E+05
922	1.1610E+05	1686	1.0246E+05
923	1.1600E+05	1687	1.0246E+05
924	1.1590E+05	1688	1.0246E+05
925	1.1580E+05	1689	1.0246E+05
926	1.1570E+05	1690	1.0246E+05
927	1.1560E+05	1691	1.0246E+05
928	1.1549E+05	1692	1.0246E+05
929	1.1539E+05	1693	1.0245E+05
930	1.1528E+05	1694	1.0246E+05
931	1.1518E+05	1695	1.0245E+05
932	1.1507E+05	1696	1.0245E+05
933	1.1496E+05	1697	1.0244E+05
934	1.1486E+05	1698	1.0244E+05
935	1.1475E+05	1699	1.0243E+05
936	1.1464E+05	1700	1.0242E+05
937	1.1453E+05	1701	1.0242E+05
938	1.1443E+05	1702	1.0241E+05
939	1.1432E+05	1703	1.0240E+05
940	1.1421E+05	1704	1.0239E+05
941	1.1410E+05	1705	1.0238E+05
942	1.1399E+05	1706	1.0236E+05
943	1.1388E+05	1707	1.0235E+05
944	1.1377E+05	1708	1.0233E+05
945	1.1366E+05	1709	1.0231E+05
946	1.1355E+05	1710	1.0229E+05
947	1.1344E+05	1711	1.0226E+05
948	1.1333E+05	1712	1.0224E+05
949	1.1322E+05	1713	1.0221E+05
950	1.1312E+05	1714	1.0218E+05
951	1.1301E+05	1715	1.0214E+05
952	1.1290E+05	1716	1.0210E+05
953	1.1280E+05	1717	1.0205E+05
954	1.1269E+05	1718	1.0200E+05
955	1.1258E+05	1719	1.0195E+05
956	1.1247E+05	1720	1.0188E+05
957	1.1237E+05	1721	1.0182E+05
958	1.1227E+05	1722	1.0175E+05
959	1.1216E+05	1723	1.0167E+05
960	1.1206E+05	1724	1.0158E+05
961	1.1196E+05	1725	1.0149E+05
962	1.1186E+05	1726	1.0138E+05
963	1.1176E+05	1727	1.0127E+05
964	1.1166E+05	1728	1.0115E+05
965	1.1156E+05	1729	1.0101E+05
966	1.1147E+05	1730	1.0087E+05
967	1.1138E+05	1731	1.0071E+05
968	1.1129E+05	1732	1.0054E+05
969	1.1120E+05	1733	1.0036E+05
970	1.1111E+05	1734	1.0016E+05
971	1.1102E+05	1735	9.9952E+04
972	1.1094E+05	1736	9.9723E+04
973	1.1086E+05	1737	9.9479E+04
974	1.1077E+05	1738	9.9217E+04
975	1.1070E+05	1739	9.8938E+04
976	1.1062E+05	1740	9.8637E+04

977	1.1055E+05	1741	9.8319E+04
978	1.1048E+05	1742	9.7978E+04
979	1.1041E+05	1743	9.7614E+04
980	1.1034E+05	1744	9.7229E+04
981	1.1028E+05	1745	9.6820E+04
982	1.1021E+05	1746	9.6388E+04
983	1.1015E+05	1747	9.5930E+04
984	1.1009E+05	1748	9.5450E+04
985	1.1004E+05	1749	9.4940E+04
986	1.0998E+05	1750	9.4400E+04
987	1.0992E+05	1751	9.3837E+04
988	1.0987E+05	1752	9.3245E+04
989	1.0982E+05	1753	9.2622E+04
990	1.0978E+05	1754	9.1968E+04
991	1.0973E+05	1755	9.1286E+04
992	1.0969E+05	1756	9.0571E+04
993	1.0965E+05	1757	8.9828E+04
994	1.0961E+05	1758	8.9048E+04
995	1.0957E+05	1759	8.8241E+04
996	1.0953E+05	1760	8.7399E+04
997	1.0949E+05	1761	8.6526E+04
998	1.0946E+05	1762	8.5622E+04
999	1.0942E+05	1763	8.4685E+04
1000	1.0938E+05	1764	8.3716E+04
1001	1.0934E+05	1765	8.2713E+04
1002	1.0930E+05	1766	8.1680E+04
1003	1.0926E+05	1767	8.0616E+04
1004	1.0921E+05	1768	7.9519E+04
1005	1.0917E+05	1769	7.8394E+04
1006	1.0912E+05	1770	7.7237E+04
1007	1.0907E+05	1771	7.6051E+04
1008	1.0902E+05	1772	7.4839E+04
1009	1.0896E+05	1773	7.3599E+04
1010	1.0890E+05	1774	7.2330E+04
1011	1.0884E+05	1775	7.1038E+04
1012	1.0878E+05	1776	6.9723E+04
1013	1.0871E+05	1777	6.8380E+04
1014	1.0863E+05	1778	6.7020E+04
1015	1.0855E+05	1779	6.5637E+04
1016	1.0846E+05	1780	6.4235E+04
1017	1.0838E+05	1781	6.2815E+04
1018	1.0828E+05	1782	6.1377E+04
1019	1.0817E+05	1783	5.9930E+04
1020	1.0806E+05	1784	5.8466E+04
1021	1.0794E+05	1785	5.6992E+04
1022	1.0781E+05	1786	5.5506E+04
1023	1.0767E+05	1787	5.4017E+04
1024	1.0751E+05	1788	5.2519E+04
1025	1.0735E+05	1789	5.1020E+04
1026	1.0717E+05	1790	4.9516E+04
1027	1.0698E+05	1791	4.8013E+04
1028	1.0677E+05	1792	4.6511E+04
1029	1.0655E+05	1793	4.5015E+04
1030	1.0630E+05	1794	4.3522E+04
1031	1.0604E+05	1795	4.2038E+04
1032	1.0576E+05	1796	4.0567E+04
1033	1.0546E+05	1797	3.9102E+04
1034	1.0514E+05	1798	3.7652E+04

1035	1.0480E+05	1799	3.6215E+04
1036	1.0443E+05	1800	3.4800E+04
1037	1.0403E+05	1801	3.3402E+04
1038	1.0361E+05	1802	3.2020E+04
1039	1.0315E+05	1803	3.0663E+04
1040	1.0267E+05	1804	2.9331E+04
1041	1.0216E+05	1805	2.8021E+04
1042	1.0161E+05	1806	2.6737E+04
1043	1.0103E+05	1807	2.5482E+04
1044	1.0042E+05	1808	2.4256E+04
1045	9.9768E+04	1809	2.3062E+04
1046	9.9084E+04	1810	2.1894E+04
1047	9.8360E+04	1811	2.0762E+04
1048	9.7599E+04	1812	1.9660E+04
1049	9.6795E+04	1813	1.8594E+04
1050	9.5952E+04	1814	1.7560E+04
1051	9.5067E+04	1815	1.6562E+04
1052	9.4141E+04	1816	1.5601E+04
1053	9.3175E+04	1817	1.4671E+04
1054	9.2163E+04	1818	1.3779E+04
1055	9.1109E+04	1819	1.2921E+04
1056	9.0009E+04	1820	1.2100E+04
1057	8.8870E+04	1821	1.1314E+04
1058	8.7685E+04	1822	1.0564E+04
1059	8.6459E+04	1823	9.8473E+03
1060	8.5194E+04	1824	9.1655E+03
1061	8.3883E+04	1825	8.5176E+03
1062	8.2534E+04	1826	7.9038E+03
1063	8.1144E+04	1827	7.3217E+03
1064	7.9715E+04	1828	6.7723E+03
1065	7.8247E+04	1829	6.2541E+03
1066	7.6748E+04	1830	5.7649E+03
1067	7.5210E+04	1831	5.3058E+03
1068	7.3649E+04	1832	4.8749E+03
1069	7.2048E+04	1833	4.4719E+03
1070	7.0419E+04	1834	4.0945E+03
1071	6.8765E+04	1835	3.7438E+03
1072	6.7090E+04	1836	3.4161E+03
1073	6.5386E+04	1837	3.1121E+03
1074	6.3668E+04	1838	2.8299E+03
1075	6.1929E+04	1839	2.5690E+03
1076	6.0182E+04	1840	2.3278E+03
1077	5.8417E+04	1841	2.1052E+03
1078	5.6648E+04	1842	1.9014E+03
1079	5.4875E+04	1843	1.7132E+03
1080	5.3097E+04	1844	1.5410E+03
1081	5.1323E+04	1845	1.3838E+03
1082	4.9550E+04	1846	1.2402E+03
1083	4.7780E+04	1847	1.1092E+03
1084	4.6021E+04	1848	9.9043E+02
1085	4.4276E+04	1849	8.8247E+02
1086	4.2550E+04	1850	7.8506E+02
1087	4.0834E+04	1851	6.9690E+02
1088	3.9143E+04	1852	6.1751E+02
1089	3.7473E+04	1853	5.4608E+02
1090	3.5829E+04	1854	4.8200E+02
1091	3.4212E+04	1855	4.2451E+02
1092	3.2629E+04	1856	3.7326E+02

1093	3.1074E+04	1857	3.2743E+02
1094	2.9557E+04	1858	2.8670E+02
1095	2.8076E+04	1859	2.5059E+02
1096	2.6629E+04	1860	2.1850E+02
1097	2.5222E+04	1861	1.9017E+02
1098	2.3857E+04	1862	1.6519E+02
1099	2.2537E+04	1863	1.4321E+02
1100	2.1257E+04	1864	1.2389E+02
1101	2.0019E+04	1865	1.0696E+02
1102	1.8827E+04	1866	9.2153E+01
1103	1.7681E+04	1867	7.9227E+01
1104	1.6578E+04	1868	6.7974E+01
1105	1.5520E+04	1869	5.8182E+01
1106	1.4508E+04	1870	4.9719E+01
1107	1.3542E+04	1871	4.2389E+01
1108	1.2619E+04	1872	3.6071E+01
1109	1.1741E+04	1873	3.0621E+01
1110	1.0907E+04	1874	2.5950E+01
1111	1.0117E+04	1875	2.1939E+01
1112	9.3675E+03	1876	1.8505E+01
1113	8.6596E+03	1877	1.5585E+01
1114	7.9930E+03	1878	1.3090E+01
1115	7.3640E+03	1879	1.0972E+01
1116	6.7737E+03	1880	9.1770E+00
1117	6.2207E+03	1881	7.6590E+00
1118	5.7034E+03	1882	6.3820E+00
1119	5.2200E+03	1883	5.3020E+00
1120	4.7685E+03	1884	4.3970E+00
1121	4.3491E+03	1885	3.6380E+00
1122	3.9600E+03	1886	3.0060E+00
1123	3.5994E+03	1887	2.4740E+00
1124	3.2656E+03	1888	2.0340E+00
1125	2.9577E+03	1889	1.6690E+00
1126	2.6737E+03	1890	1.3650E+00
1127	2.4125E+03	1891	1.1170E+00
1128	2.1733E+03	1892	9.0700E-01
1129	1.9545E+03	1893	7.3800E-01
1130	1.7539E+03	1894	5.9900E-01
1131	1.5713E+03	1895	4.8100E-01
1132	1.4052E+03	1896	3.9100E-01
1133	1.2541E+03	1897	3.1500E-01
1134	1.1172E+03	1898	2.5000E-01
1135	9.9349E+02	1899	2.0200E-01
1136	8.8171E+02	1900	1.6300E-01
1137	7.8122E+02	1901	1.2700E-01
1138	6.9049E+02	1902	1.0200E-01
1139	6.0948E+02	1903	8.1000E-02
1140	5.3684E+02	1904	6.4000E-02
1141	4.7188E+02	1905	5.1000E-02
1142	4.1403E+02	1906	3.9000E-02
1143	3.6260E+02	1907	3.0000E-02
1144	3.1688E+02	1908	2.4000E-02
1145	2.7631E+02	1909	1.7000E-02
1146	2.4054E+02	1910	1.4000E-02
1147	2.0899E+02	1911	1.1000E-02
1148	1.8123E+02	1912	7.0000E-03
1149	1.5683E+02	1913	5.0000E-03
1150	1.3544E+02	1914	4.0000E-03

1151	1.1674E+02
1152	1.0042E+02
1153	8.6220E+01
1154	7.3842E+01
1155	6.3139E+01
1156	5.3869E+01
1157	4.5868E+01
1158	3.8967E+01
1159	3.3050E+01
1160	2.7964E+01
1161	2.3617E+01
1162	1.9900E+01
1163	1.6736E+01
1164	1.4051E+01
1165	1.1766E+01
1166	9.8310E+00
1167	8.2010E+00
1168	6.8220E+00
1169	5.6660E+00
1170	4.6970E+00
1171	3.8850E+00
1172	3.2030E+00
1173	2.6370E+00
1174	2.1680E+00
1175	1.7740E+00
1176	1.4520E+00
1177	1.1870E+00
1178	9.6600E-01
1179	7.8400E-01
1180	6.3500E-01
1181	5.1400E-01
1182	4.1500E-01
1183	3.3500E-01
1184	2.6700E-01
1185	2.1600E-01
1186	1.7200E-01
1187	1.3600E-01
1188	1.0800E-01
1189	8.6000E-02
1190	6.8000E-02
1191	5.3000E-02
1192	4.2000E-02
1193	3.1000E-02
1194	2.3000E-02
1195	1.9000E-02
1196	1.3000E-02
1197	1.1000E-02
1198	6.0000E-03
1199	5.0000E-03
1200	4.0000E-03
1201	2.0000E-03
1202	0.0000E+00
1203	0.0000E+00
1915	3.0000E-03
1916	1.0000E-03
1917	0.0000E+00
1918	0.0000E+00

APPENDIX B: Determination of the uncertainty in the timing factor $\Delta f_x/f_x$

For the timing factor in Eq.(7)

$$f_x = [1-\exp(-\lambda_x t_1)]\, \Sigma_i \exp(-\lambda_x t_{2,i})\, [1-\exp(-\lambda_x t_{3,i})] \;/\; \lambda_x = \Sigma_i\, f_{x,i}\,, \quad (15)$$

the uncertainty in the timing factor is

$$\Delta f_{x,i} = (\partial f_{x,i}/\partial\lambda_x)\Delta\lambda_x = (\partial f_{x,i}\,/\,\partial\lambda_x)\,(d\lambda_x/dT_{1/2,x})\,\Delta T_{1/2,x} = (\lambda_x\,/T_{1/2,x})\,(\partial f_{x,i}/\partial\lambda_x)\,\Delta T_{1/2,x} \quad (16)$$

assuming that only the uncertainty in the half-life is responsible to the uncertainty in the timing factor. The partial derivative $\partial f_{x,i}/\partial\lambda_x$ can be calculated by

$$\partial f_{x,i}/\partial\lambda_x = f_{x,i}\, t_1 \exp(-\lambda_x t_1) \,/\, [1-\exp(-\lambda_x t_1)] - f_{x,i}\, t_{2,i}$$

$$+ f_{x,i}\, t_{3,i} \exp(-\lambda_x t_{3,i}) \,/\, [1-\exp(-\lambda_x t_{3,i})] - f_{x,i} \,/\, \lambda_x. \quad (17)$$

Finally we obtain the fractional uncertainty in f_x by

$$\Delta f_x\,/f_x = [\Sigma_i\, (\Delta f_{x,i})^2]^{1/2} \,/\, f_x, \quad (18)$$

which is listed in Table 11 as the uncertainty in the cross section due to the uncertainty in the half-life.

Nuclear Data Section
International Atomic Energy Agency
P.O. Box 100
A-1400 Vienna
Austria

e-mail: nds.contact-point@iaea.org
fax: (43-1) 26007
telephone: (43-1) 2600 21725
Web: http://www-nds.iaea.org/